

The classical and quantum synchronization between two scattering modes in Bose-Einstein condensates generated by the standing-wave laser beams

Lin Zhang^{1,*}, Xiaoting Xu¹, Xing Liu¹, and Weiping Zhang^{2,3,4†}

¹*School of physics and Information Technology, Shaanxi Normal University, Xi'an 710119, China*

²*Department of Physics and Astronomy, Shanghai Jiao Tong University, Shanghai 200240, P. R. China*

³*Quantum Institute for Light and Atoms, Department of Physics, East China Normal University, No.500, Shanghai 200241, P. R. China and*

⁴*Collaborative Innovation Center of Extreme Optics, Shanxi University, Taiyuan, Shanxi 030006, P. R. China*

Both classical and quantum dynamics of the synchronization between two nonlinear mechanical modes scattered from Bose-Einstein condensates (BECs) by the standing-wave laser beam are comparatively investigated. As the ultra-low dissipations of the momentum modes in the atomic BECs, the synchronized dynamics are studied in a framework of closed-system theory in order to track down both the classical and the quantum synchronizations from an angle of quantum control. The classical synchronization and the relevant dynamics of measure synchronization, the quantum synchronization and two different types of measures proposed by Mari and estimated by mutual information based on Q -function are studied respectively in order to reveal both the macroscopic and the microscopic signatures of synchronized behaviors in a closed quantum system. The results demonstrate that the “revival and collapse” of the quantum fluctuations beyond the classical mean-value dynamics due to long-lasting mode coherence discriminates the quantum synchronization from the classical one, which not only excludes the possibilities of an exact synchronization and a perfect density overlap in phase space, but also leads to upper limitations to Mari measure and large unceasing fluctuations to mutual information between two scattering modes. We reveal a close dynamic connection between Mari measure and the mutual information of two nonlinear momentum modes in closed BEC systems by demonstrating an opposite mean-value behavior but a similar fluctuation variation with respect to their respective evolutionary scales.

PACS numbers: 42.50.Pq, 37.10.Vz, 37.30.+i, 42.65.Pc

I. INTRODUCTION

In recent years, many attentions are paid to the quantum control problems for exploring classically driven devices which are actually working in a quantum framework [1, 2]. For the quantum control on a collection of nearly identical microscopic quantum units from a macroscopic level down to atomic/molecular scale, only the synchronized behavior emerged from the microscopic scale can be identified by the classical devices as a macroscopic signature, and thus the synchronization behaviors at the macroscopic scale, that is, the classical synchronization (CS), play a critical role to trace down (classically detect or control) the coherent quantum dynamics among the microscopic quantum units. However, the synchronized dynamics between different quantum units, which induce dynamical transitions of macroscopic temporal-spacial orders, is intrinsically determined by the microscopic synchronization within a decoherence time for a quantum evolution. Therefore, the quantum synchronization (QS) as another important signature for the quantum coherent dynamics have been extensively studied with the nanomechanical resonators [3–5], the spins and the atomic qubits [6, 7]. The dynamics of the coupled oscillators leading to QS have also been extensively considered in the optomechanical systems [8–11].

In this paper, we want to push this topic by exploring both classical and quantum natures of the synchronization between two nonlinear collective modes in a macroscopic quantum matter: Bose-Einstein condensate (BEC). In BEC, the synchronized behaviors between a large number of atoms are complicated because the dimension of BEC is huge, but the main features of synchronization can also be revealed by only analyzing the dynamics between several collective modes coherently excited from it, especially by the simplest case of a two-mode excitation. In a two-mode quantum system, one mode can be treated as a passive oscillator which is easily initialized to a ground state and the other is the active one which produces quantum control actions via their mutual couplings. In this driven-response closed loops, the dynamical measures of two quantum oscillators to be synchronized within a decoherence time are

*Electronic address: zhanglincn@snnu.edu.cn

†Electronic address: wpzhang@phy.ecnu.edu.cn

the useful signatures to guide efficient controls on the quantum evolution of the passive oscillator starting from a specific initial state. Recently, many measures are presented for the judgement of QS [12, 13] and most of the works considered two coupled nonlinear quantum oscillators exposed to different dissipative baths [14–20]. These studies are mainly concerned about QS phenomena in the open quantum systems, and the results demonstrated that QS of an open quantum system is eventually determined by the statistical properties of the external baths [21]. Further studies indicate that two oscillators coupled to a common reservoir are more likely to be synchronized than that they separately couple to two different reservoirs [22]. These dissipative synchronizations are all related to the stable steady states or the dynamical attractors to which the coupled systems can eventually settle down due to the dissipation and the decoherence induced by the baths [23]. However, for a control problem, a full real-time evolution of the correlated states between coupled units within a decoherence time is more important than the longtime asymptotic behavior. Therefore the damping and the couplings with the baths can be neglected in a short time interval which enables an assumption of a closed quantum system. As the conservation of the phase volume for a closed quantum system, the synchronization without dissipations will be very different from that of an open quantum system. In this paper, we will consider the dynamical synchronization between two autonomous nonlinear modes generated in the atomic BECs [24] by investigating the full synchronized behaviors in both the classical and the quantum regimes.

As discussed above, a complete synchronization for a closed quantum system must include both the macroscopic and the microscopic signatures of the synchronized dynamics, that is, both the CS and QS. In the classical regime, the synchronization phenomena for a dissipative system have been studied for nearly half a century from the coupled Huygens clock (in 1665) to chemical reactions, biological and social behaviors [25, 26]. Many CS measures have been proposed in different ways, such as complete synchronization, generalized synchronization, phase synchronization, lag synchronization, projective synchronization and so on [26, 27]. However, from a microscopic point of view, how to estimate QS of quantum systems is still a problem. A natural way to define a measure for QS is to generalize the classical counterparts directly to the quantum regime. However, the generalization of the classical measures to quantum case is not always straightforward because not all the classical counterparts in the quantum regime can be uniquely found, for example, the phase synchronization is related to the Hermite phase operator which, obviously, is difficult to be defined in the quantum regime [28]. While for the coupled conservative Hamiltonian systems, an interesting CS called measure synchronization (MS) was found [29] and, recently, its QS case was considered in the BEC system [30]. Up to now, two types of measure for QS are proposed in the literatures, one is based on the distance between two quantum states in the Hilbert space and the other relies on the quantum state correlations. However the distance of the quantum states in Hilbert space is not unique and different norms or inner products can be adopted for different QS definitions along this line. Moreover the QS measures defined by using state correlations are even more complicated because there exist many quantum correlations for two quantum states, such as quantum discord, quantum fidelity, quantum coherence, quantum entropy, and even different quantum entanglements [31]. Therefore, the measure to judge QS between two coupled quantum systems might not be theoretically unique and which one we should pick is only determined by what microscopic property we want to resolve. In this paper, we will investigate the dynamics of QS between two atomic scattering modes in BEC by using Q -function as a tool. As Q -function is positive and bounded, we can easily combine two types of QS measure together (the distance and the correlation) to explore the dynamical features of QS in a closed quantum system by investigating either the “distance” (overlap) from a classical aspect or the “correlation” based on the mutual information theory.

II. THE THEORETICAL MODEL

Theoretically, we consider only two low-energy scattering modes A and B stimulated in BEC by a standing-wave laser beam. The coherent atomic BEC can be prepared either in a number state or in a coherent state (see Ref.[24] for the state preparation of BEC). The Hamiltonian describing two scattering modes within a BEC beam in a number state $|N\rangle$ can be described by [24]

$$\hat{H}_N = \hat{H}_A + \hat{H}_B + \hat{H}_{AB}, \quad (1)$$

$$\hat{H}_A = \hbar\omega_A \hat{a}_A^\dagger \hat{a}_A + \hbar\chi \hat{a}_A^{\dagger 2} \hat{a}_A^2,$$

$$\hat{H}_B = \hbar\omega_B \hat{a}_B^\dagger \hat{a}_B + \hbar\chi \hat{a}_B^{\dagger 2} \hat{a}_B^2,$$

$$\hat{H}_{AB} = \hbar \left[g + \chi(\hat{N} - 1) \right] \left(\hat{a}_A^\dagger \hat{a}_B + \hat{a}_B^\dagger \hat{a}_A \right) + 4\hbar\chi \hat{a}_A^\dagger \hat{a}_A \hat{a}_B^\dagger \hat{a}_B,$$

where ω_A and ω_B are the mechanical frequencies of two momentum modes induced by the collective atomic recoil [32], $g = |\Omega|^2/4\Delta$ is the linear coupling rate with Ω being the Rabi frequency of the atom interacting with the standing-wave field and Δ being the detuning of the laser field from the atomic transition frequency, and χ is the nonlinear coupling rate which is due to the interatomic dipole-dipole interaction (photon exchange) [24, 33]. For the scattering modes generated in a BEC of number state, the total atomic number $\hat{N} = \hat{N}_A + \hat{N}_B = \hat{a}_A^\dagger \hat{a}_A + \hat{a}_B^\dagger \hat{a}_B$ is conserved in a sense of $[\hat{N}, \hat{H}_N] = 0$.

System (1) can be treated as two coupled nonlinear oscillators in Hilbert space of \mathcal{H}_N , where $\hat{H}_{A,B}$ denotes two free Kerr-like nonlinear oscillators with free energy of $\hbar\omega_{A,B} + \hbar\chi(N_{A,B} - 1)$ in a number-state representation of $\hat{N}_{A,B} |N_{A,B}\rangle = N_{A,B} |N_{A,B}\rangle$. The first term in \hat{H}_{AB} describes the mutual coupling of two nonlinear Boson oscillators which induces mode transitions and the second term of \hat{H}_{AB} describes intensity interaction analogous to two light modes in Kerr medium [20]. Surely, the above model can also be obtained in the BEC system with a double-well potential with two-mode approximation (left-well and right-well modes) [33]. Usually, for a two-mode system, an interaction picture with respect to the middle energy of $\hat{H}_0 = \frac{1}{2}\hbar(\omega_A + \omega_B)(\hat{a}_A^\dagger \hat{a}_A + \hat{a}_B^\dagger \hat{a}_B)$ can be introduced as

$$\hat{H}'_N = \hat{H}_N - \hat{H}_0 = \hbar\delta \left(\hat{a}_A^\dagger \hat{a}_A - \hat{a}_B^\dagger \hat{a}_B \right) + \hbar\chi \hat{a}_A^{\dagger 2} \hat{a}_A^2 + \hbar\chi \hat{a}_B^{\dagger 2} \hat{a}_B^2 + \hat{H}_{AB}, \quad (2)$$

where the free half-level gap between the two modes is defined by $\delta = \frac{1}{2}(\omega_A - \omega_B)$.

Surely, we can also investigate the scattering modes generated from BEC in a coherent state that is prepared by coherently mixing of several BEC beams with different atomic number of N [24]. In this sense, the above quantum system (2) can be generalized into a two-mode system in a Hilbert space of $\mathcal{H} = \bigoplus_N \mathcal{H}_N$. In the following sections we will consider both cases in the interaction picture by omitting the prime of \hat{H}'_N for simplicity.

III. NONLINEAR DYNAMICS OF CS: MEASURE SYNCHRONIZATION

Firstly, we consider the macroscopic synchronized behavior of two scattering modes in a classical point of view and the Hamiltonian system (2) admits a well-known CS: measure synchronization (MS) [29]. The operator equations for the two momentum modes in the BEC beam with a total atomic number of N will be determined by

$$i \frac{d\hat{a}_A}{dt} = \delta \hat{a}_A + g \hat{a}_B + 2\chi \left(\hat{N} + \hat{N}_B \right) \hat{a}_A + \chi \left(\hat{N} + \hat{N}_A \right) \hat{a}_B + \chi \hat{a}_B^\dagger \hat{a}_A^2, \quad (3)$$

$$i \frac{d\hat{a}_B}{dt} = -\delta \hat{a}_B + g \hat{a}_A + 2\chi \left(\hat{N} + \hat{N}_A \right) \hat{a}_B + \chi \left(\hat{N} + \hat{N}_B \right) \hat{a}_A + \chi \hat{a}_A^\dagger \hat{a}_B^2, \quad (4)$$

where $\hat{N} = \hat{N}_A + \hat{N}_B$. Equivalently, we can write it by two parts, the linear and the nonlinear parts, as

$$i \frac{d}{dt} \begin{pmatrix} \hat{a}_A \\ \hat{a}_B \end{pmatrix} = \begin{pmatrix} \delta & g \\ g & -\delta \end{pmatrix} \begin{pmatrix} \hat{a}_A \\ \hat{a}_B \end{pmatrix} + \chi \begin{bmatrix} 2 \left(\hat{N} + \hat{N}_B \right) + \hat{a}_B^\dagger \hat{a}_A & \hat{N} + \hat{N}_A \\ \hat{N} + \hat{N}_B & 2 \left(\hat{N} + \hat{N}_A \right) + \hat{a}_A^\dagger \hat{a}_B \end{bmatrix} \begin{pmatrix} \hat{a}_A \\ \hat{a}_B \end{pmatrix}.$$

If the nonlinear interatomic scattering coefficient (due to dipole-dipole interaction) $\chi = 0$, the Hamiltonian will reduce to a typical JC model with an effective Rabi frequency of $\Omega_R = \sqrt{\delta^2 + g^2}$. The nonlinear dipole-dipole coefficient χ will modify δ and g by introducing a number-dependent Kerr interaction between two momentum modes, leading to an approximate Rabi frequency of $\Omega_R \approx \sqrt{(\delta + 2\chi\hat{N})^2 + (g + \chi\hat{N})^2}$.

The classical dynamics of the two-coupled modes can be investigated by merely putting them into a coherent state of $|\alpha_{A,B}\rangle$ and just replacing $\hat{a}_{A,B} \rightarrow \alpha_{A,B}$ with $\hat{N} \rightarrow N = |\alpha_A|^2 + |\alpha_B|^2$ in Eq.(3) and Eq.(4), and then we have

$$i\dot{\alpha}(\tau) = \bar{\delta}\alpha + \bar{g}\beta + 2\chi \left(1 + |\beta|^2 \right) \alpha + \chi \left(1 + |\alpha|^2 \right) \beta + \chi\beta^*\alpha^2, \quad (5)$$

$$i\dot{\beta}(\tau) = -\bar{\delta}\beta + \bar{g}\alpha + 2\chi \left(1 + |\alpha|^2 \right) \beta + \chi \left(1 + |\beta|^2 \right) \alpha + \chi\alpha^*\beta^2, \quad (6)$$

where the normalized variables $\alpha = \alpha_A/\sqrt{N}$, $\beta = \alpha_B/\sqrt{N}$ for $|\alpha|^2 + |\beta|^2 = 1$ and the parameters $\tau = Nt$, $\bar{\delta} = \delta/N$, $\bar{g} = g/N$ are rescaled by the total atomic number of N . For a classical dynamics, the MS between two scattering modes beyond dissipation can be found in Fig.1 when the coupling rate χ enters into a certain parametric region. The right-hand column of Fig.1 shows the quadrature dynamics of $\alpha(t) = (x_A + ip_A)/\sqrt{2}$, $\beta(t) = (x_B + ip_B)/\sqrt{2}$ and the corresponding quadrature errors of

$$x_- = \frac{1}{\sqrt{2}}(x_A - x_B), \quad p_- = \frac{1}{\sqrt{2}}(p_A - p_B), \quad (7)$$

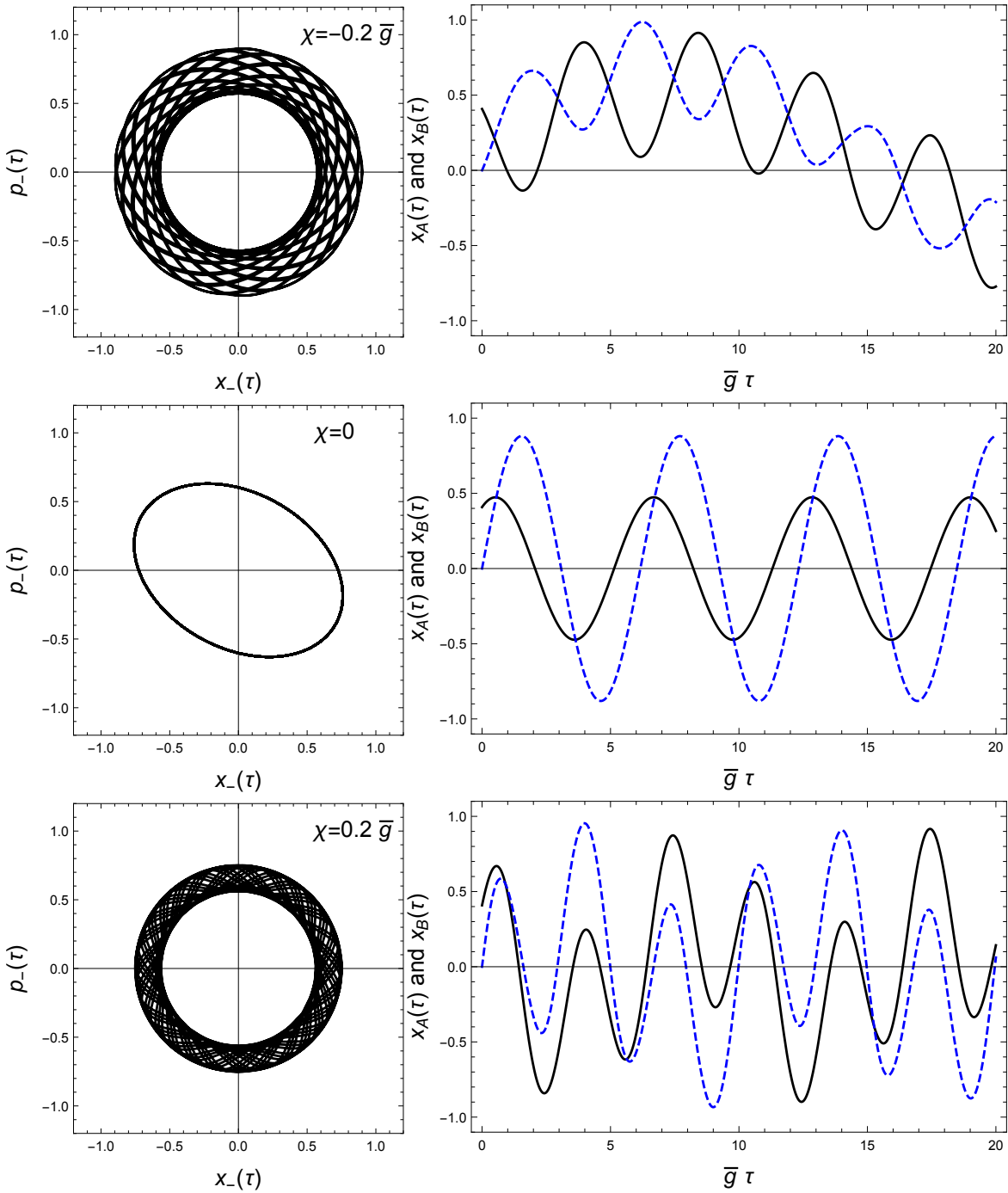


FIG. 1: The dynamics of the quadratures x_A (solid lines), x_B (dashed lines) and their corresponding errors (x_- and p_-) in the phase space under different nonlinear coupling rates $\chi = -0.2\bar{g}$ (upper panel), $\chi = 0$ (middle panel) and $\chi = 0.2\bar{g}$ (lower panel). The mode detuning is $\bar{\delta} = -0.2\bar{g}$ and the initial conditions are $\alpha(0) = (1 + 2i)/\sqrt{6}$ and $\beta(0) = i/\sqrt{6}$.

are shown in the left column in phase space. Fig.1 illustrates that the quadrature errors between modes A and B generally conduct a quasi-periodic motion and never can reach to a zero-measure orbit (a periodic circle or a constant point) in the phase space when the two modes start from different initial states, which indicates only a partial dynamical synchronization between two coupled modes without damping. As Eq.(5) and Eq.(6) are invariant for exchange of A and B , we can see a complete classical synchronization (when $x_- \rightarrow 0$ and $p_- \rightarrow 0$) only happens for $\bar{\delta} = 0$ starting from exactly the same initial states of $\alpha(0)$ and $\beta(0)$ (symmetric case). The dynamics of the two

quadratures of modes A and B perform a partial synchronization from local anti-phase motion to in-phase motion when the nonlinear coupling rate χ changes from $-0.2\bar{g}$ to $0.2\bar{g}$ as shown in the right column of Fig.1. For some specific parameters and initial states, the error dynamics will follow strict periodic orbits in the phase space with a fixed relative phase between two mechanical modes as shown in the middle panel of Fig.1 or in Fig.2(g). We notice that the local anti-phase motion of two modes covers a larger ring area of error orbit than that for a in-phase motion in the phase space, which indicates a weaker energy exchanging between two modes of synchronized motions than that of the anti-synchronized motions. As the conservation of phase volume, the separated trajectories of two modes can not run into a same orbit due to the energy exchange between them through the mode coupling. Therefore, when two modes synchronized, two interwinding trajectories are formed and they will cover the same area in the phase space since the energy exchange meets the detailed equilibrium.

The impossibility of a complete synchronization in a conservative Hamiltonian system was first investigated by Hampton and Zanette [29] and they found the interesting MS of two coupled Hamiltonian systems. Since then MS in many non-dissipative systems have been extensively studied by many authors [34–36]. As the conservation of an overall phase volume, MS exhibits a typical trajectory overlap of two coupled oscillators in the phase space. By using the polar form of a complex variables as

$$\alpha(\tau) = r_A(\tau)e^{i\theta_A(\tau)}, \beta(\tau) = r_B(\tau)e^{i\theta_B(\tau)}, \quad (8)$$

we can easily check the trajectory overlap of two scattering modes by modifying the coupling rate χ as well as the mode detuning $\bar{\delta}$ as shown in Fig.2. A typical dynamics of $r_A(\tau)$, $r_B(\tau)$ and their longtime trajectories (inset) are given in Fig.2(a). The covering areas of the quasi-periodic trajectories of modes A and B in the phase space can be estimated by

$$S_{A,B} = \pi \lim_{T \rightarrow \infty} \left(\max [r_{A,B}^2(\tau)]_T - \min [r_{A,B}^2(\tau)]_T \right),$$

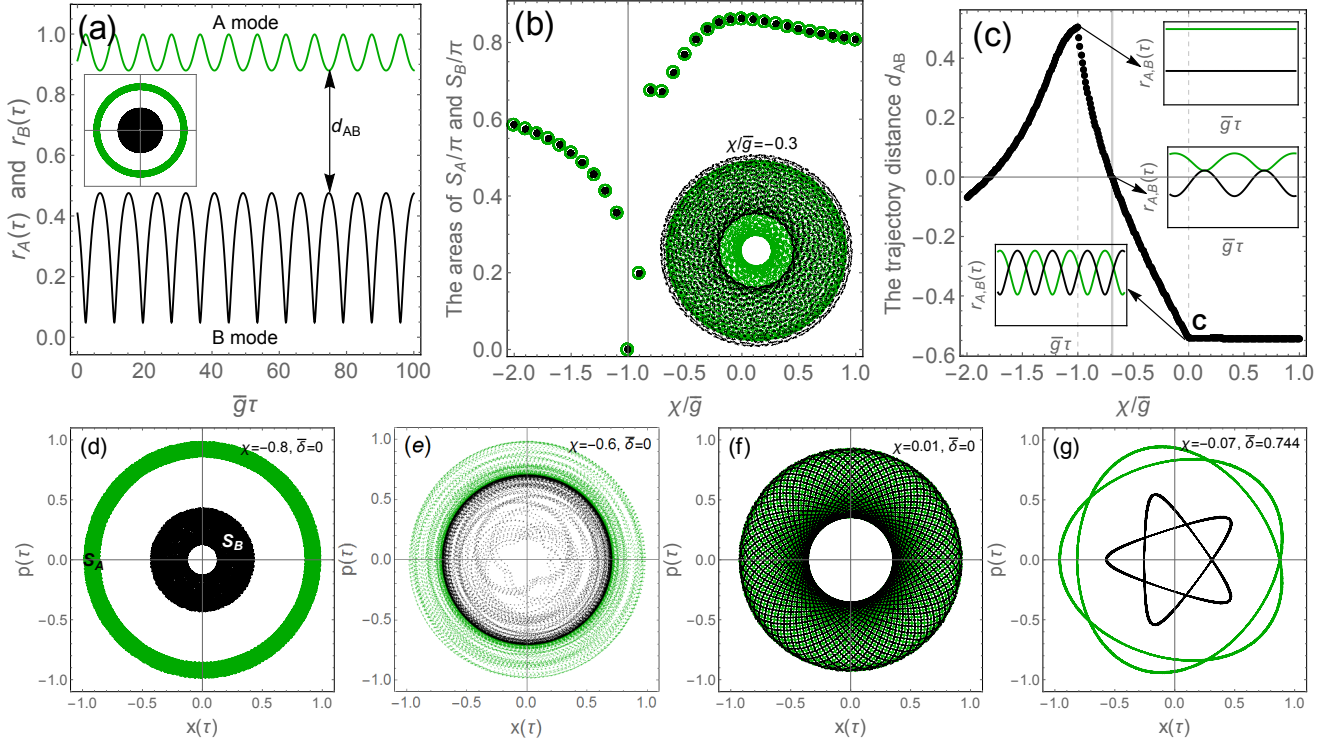


FIG. 2: (a) The temporal dynamics of $r_A(\tau)$ and $r_B(\tau)$ and the corresponding trajectories in the phase space (inset) with the parameters of $\bar{\delta} = -0.2, \chi = -0.8$; (b) The covering areas of modes A (black dots) and B (green circles) in phase space versus the coupling rate of χ under mode detuning of $\bar{\delta} = -0.4$. Inset: A sample phase picture of the trajectories in a limited time interval with $\chi/\bar{g} = -0.3$; (c) The trajectory distance between modes A and B modified by the coupling rate of χ under mode detuning of $\bar{\delta} = -1$; (d)-(f) The long-time orbital overlap in the phase space modified by the nonlinear couplings of (d) $\chi = -0.8$, (e) $\chi = -0.6$ and (f) $\chi = 0.01$ with $\bar{\delta} = 0$; (g) An accidental periodic orbit of two modes with very specific parameters of $\chi = -0.07, \bar{\delta} = 0.744$. All the parameters are scaled by \bar{g} and the initial conditions are the same as in Fig.1.

where $\max[r(\tau)]_T$ ($\min[r(\tau)]_T$) means the maximum (minimum) value of $r(\tau)$ during a time interval of T . As shown in Fig.2(b), the two modes keep nearly a same phase area ($S_A \approx S_B$ with differences below 10^{-3}) in a large parametric region of χ , displaying an invariant measure of two modes. We can also define a trajectory distance between two modes by calculating $d_{AB} = \lim_{T \rightarrow \infty} (\min[r_A(\tau)]_T - \max[r_B(\tau)]_T)$ to see the trajectory overlap in the phase space as shown in Fig.2(c). If $d_{AB} \geq 0$, the ring radius of trajectory A is larger than that of mode B and there is no overlap between them. When $d_{AB} < 0$, the overlap begins and it reaches its maximum value at a critical point C shown in Fig.2(c). Fig.2(c) reveals that the overlap of the quasi-periodic trajectories in the phase space happens only in a very specific parametric window of χ and $\bar{\delta}$, indicating the resonant exchange of energy between two scattering modes. Fig.2(d)-(f) demonstrate the trajectory overlap with the increment of coupling rate χ between two symmetric modes of $\bar{\delta} = 0$. We can find a clear evidence of orbital attraction in MS as shown in Fig.2(c) for that the orbital merging is more quickly than orbital separation with respect to the coupling rate of χ (the slope of d_{AB} dramatically decreases at the point of C in Fig.2(c)). For some specific initial states and parameters, the trajectories of modes A and B will run into the interesting synchronized periodic orbits (the correlated Lissajous curves with zero measures) such as shown by Fig.2(g). We can numerically verify that there are many correlated Lissajous orbits in the phase space determined by the initial conditions and the parameters of χ and $\bar{\delta}$. Therefore, according to the classical dynamics of Eq.(5) and Eq.(6), the two nonlinear scattering modes can obtain a partial synchronized dynamics in certain parametric windows in a sense of covering the same phase space of their trajectories with invariant measures or conducting correlated Lissajous orbits with zero measures.

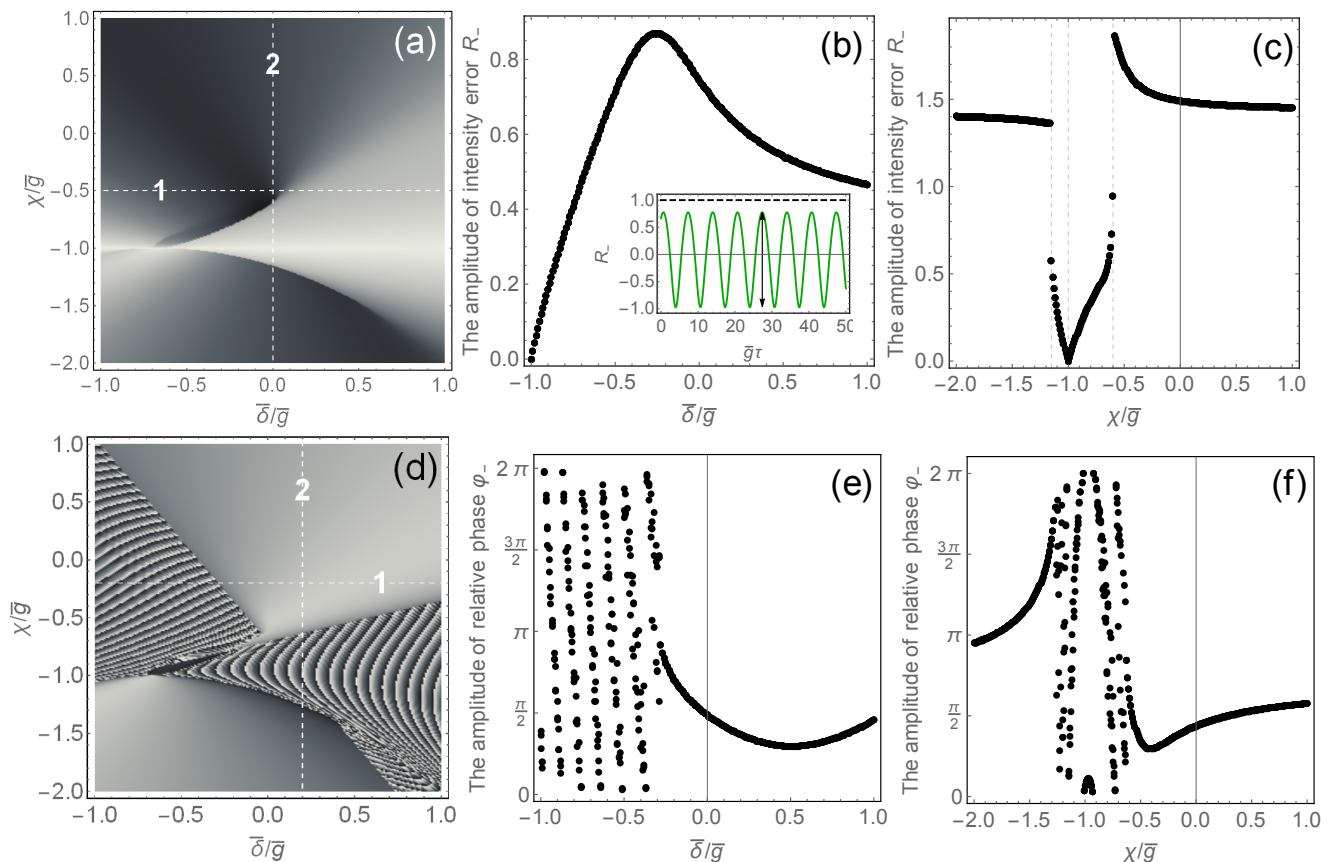


FIG. 3: The amplitudes of R_- and φ_- of the two mechanical modes modified by $\bar{\delta}$ and χ . (a) The density plot of the amplitude of $R_-(\tau)$ in the plane of $\bar{\delta}$ and χ ; The amplitude of $R_-(\tau)$ changes with (b) $\bar{\delta}$ or with (c) χ under the specific coupling $\chi = -0.5$ or detuning $\bar{\delta} = 0$ indicated by the dashed line 1 and 2 in (a); (d) The density plot of amplitude of phase difference φ_- in the plane of $\bar{\delta}$ and χ ; (e)(f) The amplitude of φ_- versus $\bar{\delta}$ or χ for fixed $\chi = -0.2$ or $\bar{\delta} = 0.2$. All the frequencies are scaled by \bar{g} and the initial conditions are set to be the same as those in the previous figures.

As for a non-dissipative Hamiltonian system, the trajectory should be very sensitive to the initial conditions because the total phase volume of two coupled systems is determined by the initial states. The synchronized behavior of MS can exhibit a different characteristic if we consider the dynamics via intensity imbalance and relative phase between two modes starting from different initial states. Then the trajectory overlap means that two scattering modes can

possess a correlated intensity relation or lock to a constant relative phase as implied by Fig.1 and Fig.2. The instantaneous intensity imbalance and phase difference between two mechanical modes can be defined by

$$R_- = |\alpha|^2 - |\beta|^2 = r_A^2 - r_B^2, \quad \varphi_- = \arg(\alpha) - \arg(\beta) = \theta_A - \theta_B. \quad (9)$$

As a general quasi-periodic behavior of $R_-(\tau)$ (see the inset of Fig.3(b)), the oscillating amplitude of $R_-(\bar{\delta}, \chi, \tau)$ changing with the detuning $\bar{\delta}$ and χ is calculated in Fig.3(a). Fig.3(b) and Fig.3(c) are the oscillating amplitudes of R_- with respect to $\bar{\delta}$ and χ for the specific $\chi = -0.5$ and $\bar{\delta} = 0$, respectively, indicated by the dashed lines of 1 and 2 in Fig.3(a). Fig.3(a) reveals that the amplitude of the intensity imbalance can reach a constant value (AC behavior) and it will disappear for $\chi = -\bar{g}$ or at a large value of $\bar{\delta}$ (DC behavior). Similarly, the amplitudes of the relative phase $\varphi_-(\tau)$ are also shown in the lower frames of Fig.3. Fig.3(d) presents the density plot of oscillating amplitude of $\varphi_-(\tau)$ in the parametric plane of $\bar{\delta}$ and χ . Fig.3(e) and (f) display the amplitudes of $\varphi_-(\tau)$ changing with respect to parameters $\bar{\delta}$ and χ indicated by two dashed lines of 1 and 2 in Fig.3(d), respectively. We can see that, in some parametric windows of $\bar{\delta}$ and χ , the oscillating amplitude of $\varphi_-(\tau)$ is randomly dependent on the parameters. Fig.3(d)-(f) demonstrate that only in specific parametric windows of $\bar{\delta}$ and χ can the phase amplitude obtain a stable value for a partial phase synchronization.

Alternatively, the intensity imbalance or the phase error being an indicator of the MS [29] can be revealed by the equations of

$$\dot{r} = -(\bar{g} + \chi)(r^2 + 1) \sin \varphi_-, \quad (10)$$

$$\dot{\varphi}_- = -2\bar{\delta} + 2\chi \frac{r^2 - 1}{r^2 + 1} + (\bar{g} + \chi) \left(r - \frac{1}{r} \right) \cos \varphi_-, \quad (11)$$

where we introduce the amplitude ratio of $r = r_A/r_B$ as a convenient variable to describe the amplitude balance between two mechanical modes with a number conservation of $r_A^2 + r_B^2 = 1$. We can easily verify that $R_- = (r^2 - 1)/(r^2 + 1)$ and a fixed amplitude synchronization for $r_A(\tau) \propto r_B(\tau)$ only happens when $\chi = -\bar{g}$ or $\varphi = n\pi, n \in \mathbb{Z}$. In the case of $\chi = -\bar{g}$, the solution for the relative phase will be $\varphi_-(t) = \varphi_0 + 2(\chi R_0 - \bar{\delta})t$, $R_-(0) \equiv R_0 = (r_0^2 - 1)/(r_0^2 + 1)$, where the initial vales $r_0 = r(0)$ and $\varphi_0 = \varphi_-(0)$. Specifically, $R_0 = \bar{\delta}/\chi$ is a steady state of Eq.(10) and (11) under $\chi = -\bar{g}$ for $\varphi_- = \varphi_0$. For $\varphi = n\pi$, a quartic equation of r should be solved to get the steady states in this case (the complete synchronization is related to the stable steady states corresponding the fixed points shown in Fig.4). Fig.4 displays the orbits in the phase space of (φ_-, R_-) with random initial r_0 and φ_0 when the frequency detuning $\bar{\delta}$ changes from negative to positive. The orbital flow in the phase space indicates that the amplitude synchronization or the phase synchronization only happens under specific initial conditions, such as $R_-(0) = \pm 1$ or $\varphi_-(0) = \pi/2, 3\pi/2$ as shown in Fig.4 by the separatrices (thick black lines). The phase transitions from self-trapping case on mode A in Fig.4(a) to the tunneling case in Fig.4(b) and to the self-trapping case on mode B in Fig.4(c) are all connected by the asymptotic synchronization lines passing through the same dynamical frustrated points of $\varphi_- = \pi/2$ and $\varphi_- = 3\pi/2$ ($R_- = \pm 1$). The trajectory flow shown in Fig.4 reveals that only a partial phase synchronization can

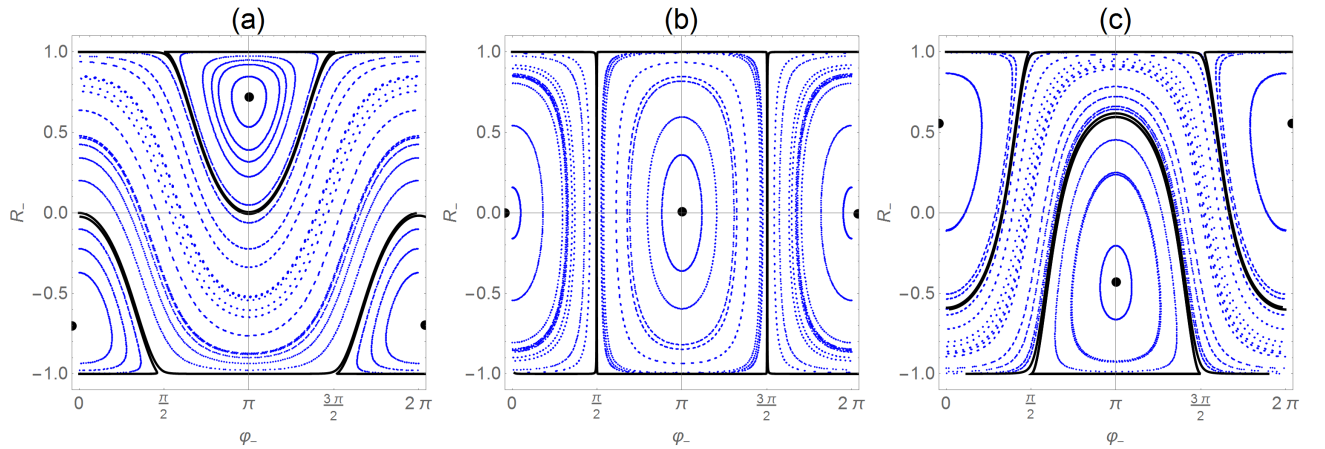


FIG. 4: The evolutions of the intensity imbalance R_- and phase difference φ_- in the phase space with (a) $\bar{\delta} = -1$, (b) $\bar{\delta} = 0$ and (c) $\bar{\delta} = 0.5$, starting from the random initial conditions. The mode coupling rate is $\chi = -0.01$ and all the frequencies are scalded by \bar{g} . The thick black lines are the separatrices of the orbits and the black dots are the stable steady states.

easily be obtained for $\bar{\delta} = 0$ (Fig.4(b)) and the exact synchronized motion between two conservative modes is indeed an accidental case corresponding only to the stable steady states which can be shared by both modes.

As described in Ref.[29], a complete CS that two different orbits of the system collapse into the same one is impossible in the coupled Hamiltonian systems because the phase volume must be preserved (no damping). However, a weak or partial synchronization can be established between two coupled conservative modes with a signature of two attractive interwinding orbits formed in phase space due to mutual exchange of energy. According to the above calculations on mean-value dynamics, we see that the partial two-mode synchronized motion can safely be acquired through the mode coupling under specific parametric conditions in a MS point of view. If the initial conditions are specially chosen, a full synchronization to reach the stable steady states can still be realized in this system classically. However, in order to consider the synchronization from a quantum aspect, we should give up the trajectory picture to investigate the probability density distribution in the phase space instead. Recently, a work studied the MS in a quantum regime to reveal some quantum properties of two coupled modes in BEC system [30]. As the fluctuations are always involved in the quantum dynamics, the CS measure by just investigating the overlap of the mean-value trajectories in the phase space is obviously too rough for a quantum dynamics.

IV. THE COHERENT DYNAMICS OF QUANTUM SYNCHRONIZATION

A. QS of scattering modes from BEC in a number state

Because of the intrinsic fluctuations in a quantum system, the QS is essentially different from the classical one and a complete synchronization of two coupled quantum modes is definitely avoided due to the uncertainty principle. In order to show the dynamics of QS in a closed quantum system, the total state of two excited modes in BEC should follow the Schrödinger equation of

$$i\hbar \frac{d}{dt} |\psi(t)\rangle = \hat{H}_N |\psi(t)\rangle, \quad (12)$$

where the wave function $|\psi(t)\rangle$ in the Hilbert space of \mathcal{H}_N can be expanded by

$$|\psi(t)\rangle = \sum_{j=0}^N C_j(t) |j, N-j\rangle, \quad (13)$$

whose form is due to the conservation of N (N denotes the total atomic number of BEC in number state $|N\rangle$ and thus the dimension of \mathcal{H}_N is $D = N + 1$) and the unitary evolution keeps $\sum_{j=0}^N |C_j(t)|^2 = 1$. Substituting Eq.(13) into Eq.(12), we have the equation of motion for the coefficients $C_j(t)$ as

$$i\dot{C}_j(t) = \sqrt{j(N-j+1)} [g + \chi(N-1)] C_{j-1}(t) + [\chi N^2 - (\chi + \delta)N + 2j(\delta + \chi N) - 2\chi j^2] C_j(t) + \sqrt{(j+1)(N-j)} [g + \chi(N-1)] C_{j+1}(t). \quad (14)$$

Clearly, the above coupled equations produce a symmetric tridiagonal matrix of Hamiltonian \hat{H}_N in the Fock representation and the algorithm to calculate its eigenvalues are well-known (e.g., bisection algorithm [37]). Fig.5 gives a simple case of energy levels for BEC with only 3 atoms ($D = 4$) modified by the nonlinear couplings of χ . There are four energy levels in this case whose eigenstates are the superposition of four bare number states of $|0, 3\rangle$, $|1, 2\rangle$, $|2, 1\rangle$ and $|3, 0\rangle$. Clearly, the population distributions of modes A and B are dynamically determined by the avoided level crossings of the states which can easily be modified by δ and χ . A clear degenerate case of $g + \chi(N-1) = 0$ shown in Fig.5(b) indicates a transitionless evolution between four bare states without energy avoided crossings for

$$C_j(t) = C_j(0) e^{-i[\chi N^2 - (\chi + \delta)N + 2j(\delta + \chi N) - 2\chi j^2]t}. \quad (15)$$

This corresponds to the classical case of $\chi = -\bar{g} \equiv -g/N$ for a synchronized intensity balance (see Eq.(10) for $\dot{r} = 0$) that only the relative phase is linearly increasing just like that in Eq.(15).

Actually, an overlap of the quantum dynamics of modes A and B in the phase-space should be investigated by using the probability distributions of the total quantum states. The Q -function based on the coherent state representation possesses a good behavior to provide positive and bounded probability distributions in the phase space. The coherent properties of a quantum state $|\psi(t)\rangle$ can be revealed by a continuous function which is a projection of the quantum state onto a reference coherent state $|\alpha\rangle$ by $\psi(\alpha, t) = \langle \alpha | \psi(t) \rangle$, and its probability density is called Q -function as

$$Q(\alpha, t) = |\psi(\alpha, t)|^2,$$

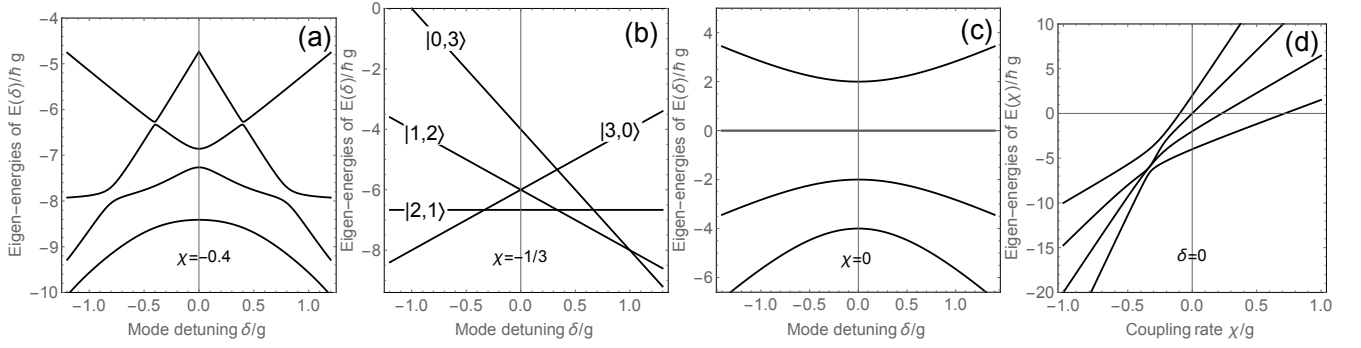


FIG. 5: The energy levels of the BEC modes of 3 atoms changing with different nonlinear couplings of (a) $\chi = -0.4$, (b) $\chi = -1/3$, (c) $\chi = 0$, and with (d) $\delta = 0$.

If the Q -function goes to 1 in the phase space, then the state $|\psi(t)\rangle$ will be completely described by a coherent state $|\alpha\rangle$ with an overall amplitude and phase. Therefore, the quantum MS of two quantum states can then be traced by the overlap of probability distributions in the phase space revealed by Q -function. The Q -function for the two-mode state of BEC in a number state $|N\rangle$ is

$$Q_N(\alpha_A, \alpha_B, t) = \langle \alpha_A, \alpha_B | \hat{\rho}_N | \alpha_A, \alpha_B \rangle = |\langle \alpha_A, \alpha_B | \psi(t) \rangle|^2, \quad (16)$$

where the density operator $\hat{\rho}_N = |\psi(t)\rangle\langle\psi(t)|$. In terms of $C_j(t)$, the above Q -function can be written as

$$Q_N(\alpha_A, \alpha_B, t) = \left| \sum_{j=0}^N C_j(t) \frac{(\alpha_A^*)^j (\alpha_B^*)^{N-j}}{\sqrt{j!(N-j)!}} \right|^2 e^{-(|\alpha_A|^2 + |\alpha_B|^2)} \geq 0. \quad (17)$$

By using Cauchy's inequality for a certain N , the above Q -function has an upper limit function of

$$Q_N(\alpha_A, \alpha_B, t) \leq \frac{1}{N!} \left(|\alpha_A|^2 + |\alpha_B|^2 \right)^N e^{-(|\alpha_A|^2 + |\alpha_B|^2)} \equiv \bar{Q}_N, \quad (18)$$

where the normalization condition in the Hilbert space \mathcal{H}_N is used. Clearly, the above bounded Q -function \bar{Q}_N gives a central symmetric distribution for modes α_A and α_B and no phase information is included.

The detailed evolution of the Q -function can be tracked down by exactly solving coefficients of C_j s of Eq.(14) under certain initial conditions. As the total atomic number N is conserved in the space of \mathcal{H}_N , the initial condition for A mode is assumed to be in the ground number state and B mode is in a vacuum state, that is, $|\psi(0)\rangle = |N\rangle_A \otimes |0\rangle_B = |N, 0\rangle$ for $C_j(0) = 0, j = 0, \dots, N-1$ and $C_N(0) = 1$. Then the initial two-mode Q -function is

$$Q_N(\alpha_A, \alpha_B, 0) = \frac{\left(|\alpha_A|^2 \right)^N}{N!} e^{-(|\alpha_A|^2 + |\alpha_B|^2)}, \quad (19)$$

which gives two well-separated probability distributions of two modes with no overlap in the phase space as shown in Fig.6 ($t = 0$). The evolution of the probability distributions in the phase space with $N = 15$ for modes A and B are subsequently shown in Fig.6. As the high dimension of $Q(\alpha_A, \alpha_B, t)$, only the joint distributions of one-mode with a specific value of the other can be depicted in Fig.6. The main property shown in Fig.6 is that the local overlaps of the phase distributions can be obtained during the state evolution, and a transient complete overlap can reach at a certain time (e.g. $t = 1$ in Fig.6). The gradually merging of distributions of modes A and B in the phase space indicates that only a partial QS can be maintained between two coupling modes in a Hilbert space of \mathcal{H}_N after a long time evolution. Surely, the imperfect overlaps of the phase distributions can be enhanced by properly adjusting the coupling rate of χ and the frequency detuning δ as well as the initial states of two modes. As Fig.6 only shows temporal joint distributions for one mode when the other one is in a specific value, so a marginal single-mode quasi-probability

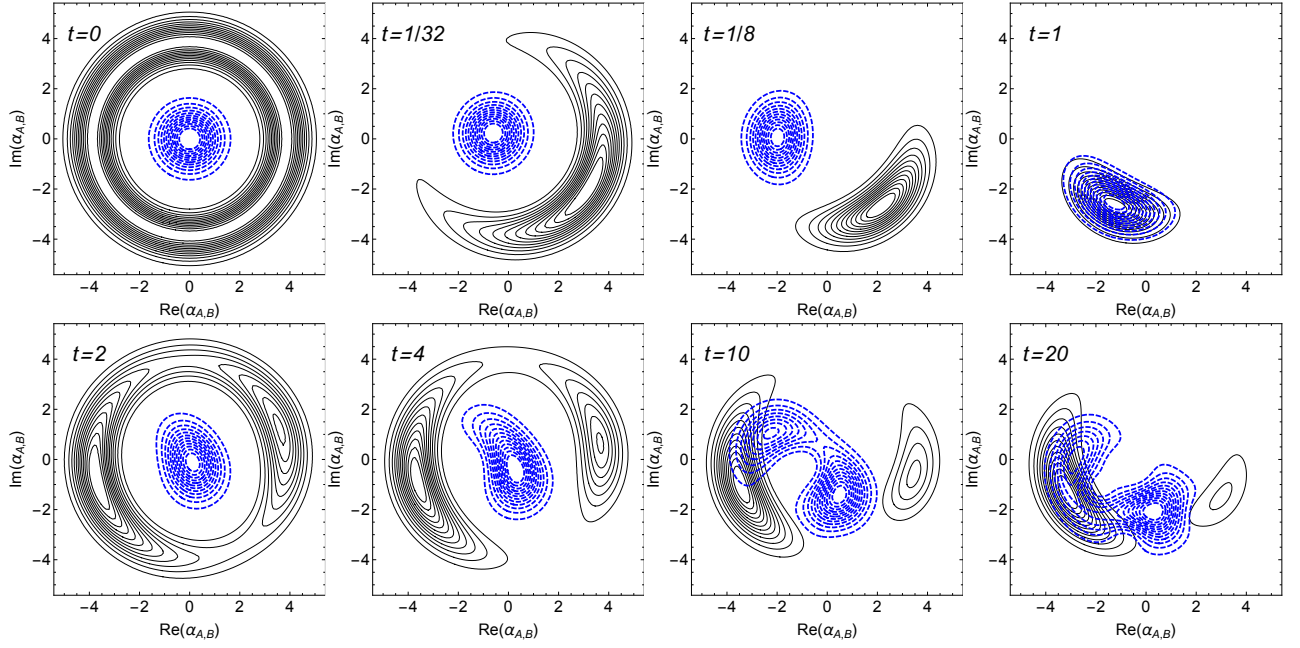


FIG. 6: The temporal density distributions of the Q -functions for two modes $Q(\alpha_A, \alpha_B, t)$ with specific $\alpha_B = 1 + 2i$ (solid lines) or with specific $\alpha_A = 1 + 2i$ (dashed lines) at different evolution times t . The parameters are $\chi/g = -0.01$ and $\delta/g = -1$. The time unit of the evolution is $\pi/[1 + (N-1)\chi/g]$.

function of A or B can be achieved by integrating all the values of the other

$$Q(\alpha_A, t) = \int Q(\alpha_A, \alpha_B, t) \frac{d^2\alpha_B}{\pi} = e^{-|\alpha_A|^2} \sum_{j=0}^N \Gamma\left(N - j + \frac{1}{2}\right) |C_j(t)|^2 \frac{(|\alpha_A|^2)^j}{j!(N-j)!}, \quad (20)$$

$$Q(\alpha_B, t) = \int Q(\alpha_A, \alpha_B, t) \frac{d^2\alpha_A}{\pi} = e^{-|\alpha_B|^2} \sum_{j=0}^N \Gamma\left(j + \frac{1}{2}\right) |C_j(t)|^2 \frac{(|\alpha_B|^2)^{N-j}}{j!(N-j)!}. \quad (21)$$

The above results clearly show that the marginal Q -functions for A and B modes produce symmetric circular distributions which conduct breathing motions in the phase space as shown in Fig.7. The breathing modes of the ringlike distribution mask all the irregular details of distribution patterns induced by the nonlinear dynamics of two coupling modes. Although no stable distribution can be reached beyond dissipations, a correlated out-of-phase breathing motion of the ring distributions of A and B is revealed and a transient perfect overlap of the marginal Q -functions at certain time ($t = 1$) is also found. The dynamics of the probability distributions demonstrated by the marginal Q -functions in Fig.7 also verifies the partial QS behavior between two scattering momentum modes in BEC.

In order to reveal the avoidance of a perfect QS between two scattering modes generated in the BEC, we can investigate the error (or deviation) operators between A and B modes defined by

$$\begin{aligned} \hat{x}_- &= \frac{1}{\sqrt{2}} (\hat{x}_A - \hat{x}_B) \equiv \frac{1}{\sqrt{2}} \left[(\hat{a}_A^\dagger + \hat{a}_A) - (\hat{a}_B^\dagger + \hat{a}_B) \right], \\ \hat{p}_- &= \frac{1}{\sqrt{2}} (\hat{p}_A - \hat{p}_B) \equiv \frac{i}{\sqrt{2}} \left[(\hat{a}_A^\dagger - \hat{a}_A) - (\hat{a}_B^\dagger - \hat{a}_B) \right], \end{aligned}$$

where the zero-point-of-fluctuation units of $x_{\text{zpf}}^{A,B} = \sqrt{\frac{\hbar}{2m_{A,B}\omega_{A,B}}}$ and $p_{\text{zpf}}^{A,B} = \sqrt{\frac{\hbar m_{A,B}\omega_{A,B}}{2}}$ for quadratures of modes A, B ($\hat{x}_{A,B}$ and $\hat{p}_{A,B}$) are used respectively. Then the error operators obey $[\hat{x}_-, \hat{p}_-] = 2i$ and which leads to a fluctuation uncertainty for any quantum state in the Hilbert space as

$$\sigma^2(x_-) \sigma^2(p_-) \geq \left(\frac{1}{2i} \langle [\Delta\hat{x}_-, \Delta\hat{p}_-] \rangle \right)^2 = \left(\frac{1}{2i} \langle [\hat{x}_-, \hat{p}_-] \rangle \right)^2 = 1, \quad (22)$$

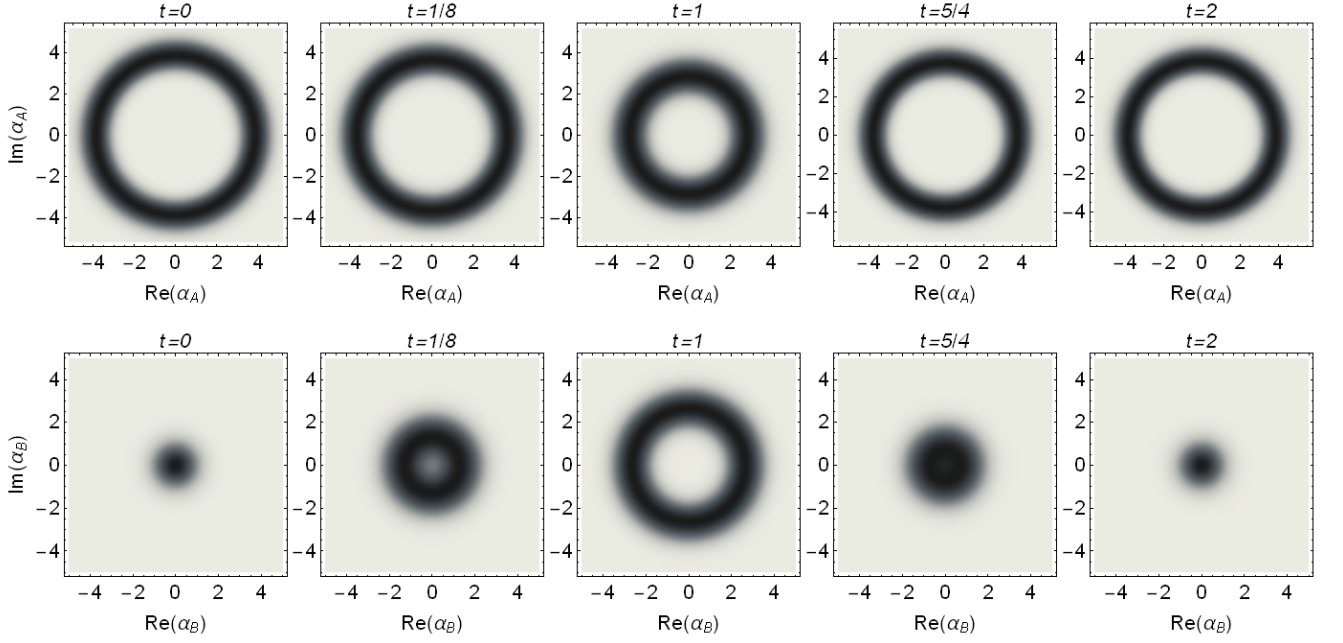


FIG. 7: The reversed dynamical phase distributions of two modes revealed by marginal Q -functions $Q(\alpha_A, t)$ (upper panel) and $Q(\alpha_B, t)$ (lower panel) with the same parameters, time scale and initial conditions as that in Fig.6.

where the deviation of an arbitrary operator \hat{O} is defined by $\Delta\hat{O} \equiv \hat{O} - \langle\hat{O}\rangle$, its variance is $\sigma^2(O) \equiv \langle(\Delta\hat{O})^2\rangle$ and the fluctuation above mean value is characterized by $\sigma(O) \equiv \sqrt{\langle(\Delta\hat{O})^2\rangle}$. The inequality of Eq.(22) indicates that if one quadrature ($\hat{x}_{A,B}$) of the two modes is synchronized ($\hat{x}_- \rightarrow 0$), then the other ($\hat{p}_{A,B}$) will diverge, which means that a complete QS between two coupled modes is impossible in quantum regime. As the quantum states in a closed Hilbert space of \mathcal{H}_N are always on a pure states following Schrödinger equation, the uncertainty of fluctuation will always plays the role to destroy the dynamical synchronization between two modes in quantum regime.

In order to reveal why two nonlinear classical oscillators can synchronize completely via their mutual couplings but, in the quantum regime, they never do, we now consider the dynamics of the error operators with both the mean values and their variances, simultaneously. The classical dynamics of the two modes are always characterized by the mean values of their positions $x_A \equiv \langle\hat{x}_A\rangle, x_B \equiv \langle\hat{x}_B\rangle$ and momenta $p_A \equiv \langle\hat{p}_A\rangle, p_B \equiv \langle\hat{p}_B\rangle$, and, often, the CS is estimated only by

$$x_-(t) = \frac{1}{\sqrt{2}} [x_A(t) - x_B(t)], \quad p_-(t) = \frac{1}{\sqrt{2}} [p_A(t) - p_B(t)], \quad (23)$$

because the higher-order correlations decays very quickly with respect to the classical time scale and the variances are always much smaller than the mean values in a real system. Therefore, a complete CS is only estimated by a vanishing of the mean errors after a longtime evolution. A partial synchronization, such as the phase or amplitude synchronization, is achieved when the differences between amplitudes of $R_{A,B} = x_{A,B}^2(t) + p_{A,B}^2(t)$ or the phases of $\varphi_{A,B}(t) = \tan^{-1} [p_{A,B}(t)/x_{A,B}(t)]$ are finally locked to a constant value, i.e., the deviation

$$R_- = R_A(t) - R_B(t) \quad \text{or} \quad \varphi_-(t) = \varphi_A(t) - \varphi_B(t)$$

asymptotically converges to a constant of $R_0 \geq 0$ or $\varphi_0 \in [0, 2\pi]$ (see Fig.4).

However, for a quantum dynamics in a closed system, the high-order coherence of the error operators should be included for a full synchronization judgement, which will lead non-negligible modulations to the mean-value dynamics between two modes. The fluctuations of the error operators beyond mean values can be estimated by

$$\sigma(x_-) = \frac{1}{\sqrt{2}} \sqrt{\sigma^2(x_A) + \sigma^2(x_B)}, \quad (24)$$

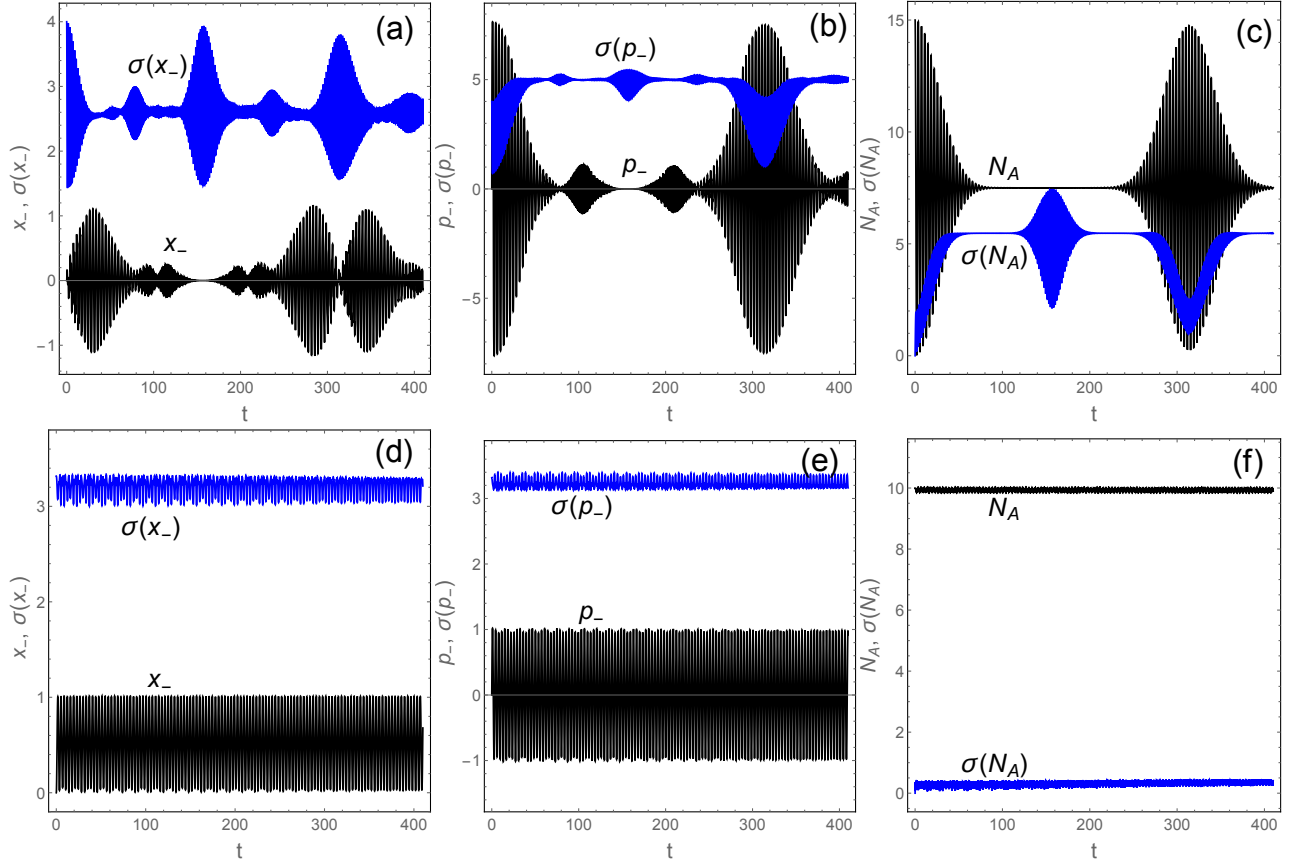


FIG. 8: The dynamics of mean values and their relevant uncertainties for (a) (b) (c) $N = 15$ in the symmetric case of $\delta = 0$ and $\chi/g = -0.01$, and (d) (e) (f) for $N = 10$ with $\delta = 0$ and $\chi/g = -0.1$. The initial condition is determined by Eq.(19).

where $\sigma^2(x_A)$ and $\sigma^2(x_B)$ are position variances for modes A and B , and

$$\sigma(p_-) = \frac{1}{\sqrt{2}} \sqrt{\sigma^2(p_A) + \sigma^2(p_B)}, \quad (25)$$

where $\sigma^2(p_A)$ and $\sigma^2(p_B)$ are their momentum variances. Fig.8 shows the mean-value dynamics of the error operators and their corresponding fluctuations in a parametric region where the partial CS in Fig.3 occurs. Fig.8(a)(b) indicate that the varying fluctuations over the mean-value dynamics sometimes plays a dominant role in the dynamics. We can see that the error fluctuations become very large at the “revival times” that introduce large deviations of x_- and p_- to destroy the mean-value synchronization between two modes. Both error quadratures conduct revival and collapse dynamics due to coherent superpositions of different mode frequencies of $C_j(t)$, $j = 0, 1, \dots, N$. The mode number of $N_A \equiv \langle \hat{N}_A \rangle = \sum_{j=0}^N j |C_j|^2$ also exhibits a collapse and revival dynamics and the number fluctuations increase during the collapse region and depresses during the revival period of time (see Fig.8(c)).

We can find a quantum trapping case of this model that, if the coupling parameter satisfies $\chi = -g/(N-1)$, all the non-diagonal terms in Eq.(14) vanish and the quantum state will confine to the initial Fock state $|N, 0\rangle$ because it is the eigenstate of the total Hamiltonian. Surely, this case is demanding and accidental because any fluctuations on the parameters will destroy it and the transition from initial state to other states will be activated. However, if $g + (N-1)\chi \rightarrow 0$, the oscillating amplitudes and frequencies of $C_j(t)$ will be dramatically decreased and the fluctuations of all the variables will be suppressed. Fig.8(d)-(f) demonstrate this case for $N = 10$ giving $g + (N-1)\chi = 0.1$ and we can see a clear suppression of varying amplitudes of the mean values and their variances, both of them losing the manifest “collapse and revival” behaviors compared with that in Fig.8(a)-(c).

Because of the unceasing coherent revival of the quantum fluctuations, QS is anyway different from its classical counterpart. In order to compare CS with QS, Mari et. al. [12] introduced a generalized criterion which is based on

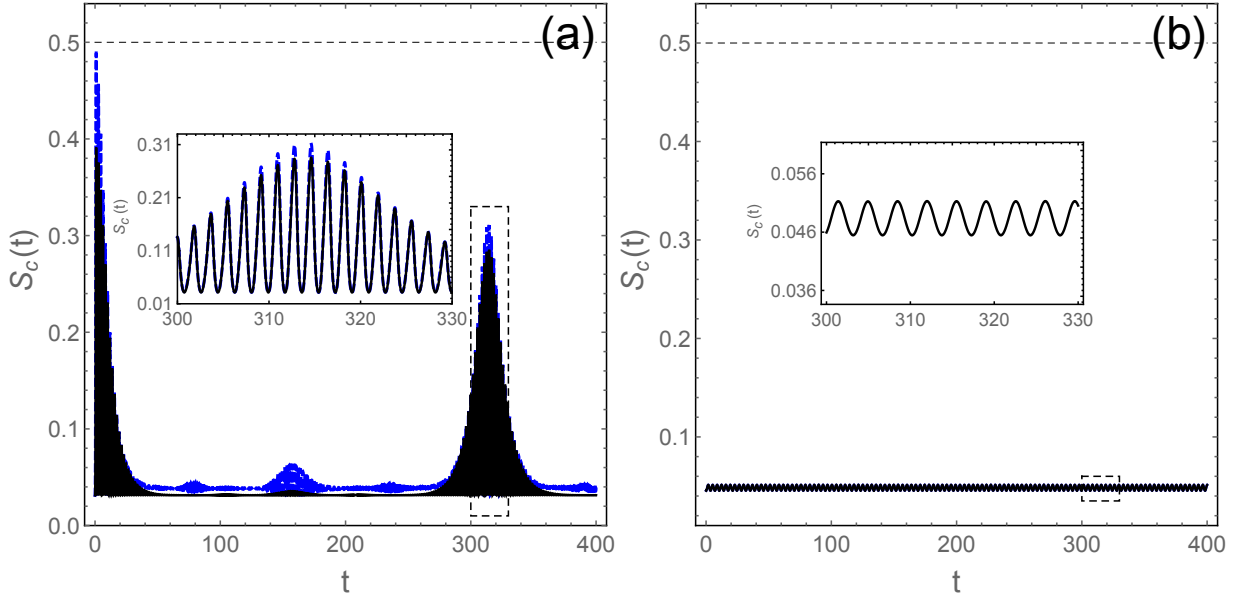


FIG. 9: The dynamical measure of synchronization $S_c(t)$ for different subspace of (a) $N = 15$ and (b) $N = 10$ with the same parameters as in Fig.8. Insets: the zoomed-in images of $S_c(t)$ from the dashed rectangles.

the fluctuations of the error operators as

$$S_c(t) \equiv \frac{1}{\sigma^2(x_-) + \sigma^2(p_-)} = \frac{1}{\langle (\Delta \hat{x}_-)^2 + (\Delta \hat{p}_-)^2 \rangle}.$$

This quantity gives the orbital deviation between two modes in the classical field and can measure the level of QS with a quantum limit of

$$S_c(t) \leq \frac{1}{2\sqrt{\langle (\Delta \hat{x}_-)^2 \rangle \langle (\Delta \hat{p}_-)^2 \rangle}} \leq \frac{1}{2}. \quad (26)$$

In the classical dynamics, $S_c(t)$ is unbounded for a regular classical orbit in the phase space (no deviation fluctuations) and will easily break the upper limit of 1/2 such as in an irregular orbit of chaotic state. Fig.9 demonstrates $S_c(t)$ with a limits of Eq.(26) in the model of two scattering modes of BEC in different number states of N . Clearly, the upper limit of 1/2 holds safely during the quantum dynamics and the measure $S_c(t)$ is closely below the quantum uncertainty limitation: the middle term of Eq.(26) (the dashed blue curves in Fig.9). Fig.9(b) is for the trapping case of $g + (N - 1)\chi = 0.1$. The calculation verifies that the quantum fluctuation is a permanent property of quantum dynamics and always exclude a full QS between the coupled quantum systems.

Recently, Ameri et al. [13] demonstrated that the fluctuation measure of $S_c(t)$ has a similar behavior to the coherent measure of the mutual information for modes A and B , which, in a steady state case, can be defined by

$$I = S(\hat{\rho}_A) + S(\hat{\rho}_B) - S(\hat{\rho}),$$

where the Von Neumann entropy $S(\hat{\rho}) = -Tr(\hat{\rho} \ln \hat{\rho})$ and $\hat{\rho}_{A,B} = Tr_{B,A}(\hat{\rho})$. In our present model, the density operator is time-dependent and can then be given by

$$S(\hat{\rho}) = -Tr(\hat{\rho} \ln \hat{\rho}) = -\sum_j \lambda_j(t) \ln \lambda_j(t),$$

where $\lambda_j(t)$ is the transient eigenvalue of the density operator. As the present quantum system will keep a unitary evolution in the absence of dissipation, the entropy reduces to $S(\hat{\rho}) = 0$, $S(\hat{\rho}_A) = S(\hat{\rho}_B)$, and the mutual information becomes $I(t) = 2S(\hat{\rho}_A)$. Now we introduce the mutual information expressed by Q -function to investigate the dynamical synchronization of two quantum modes as

$$I_{AB}(t) = \int \int Q(\alpha_A, \alpha_B, t) \ln \left[\frac{Q(\alpha_A, \alpha_B, t)}{Q(\alpha_A, t) Q(\alpha_B, t)} \right] \frac{d^2 \alpha_A}{\pi} \frac{d^2 \alpha_B}{\pi},$$

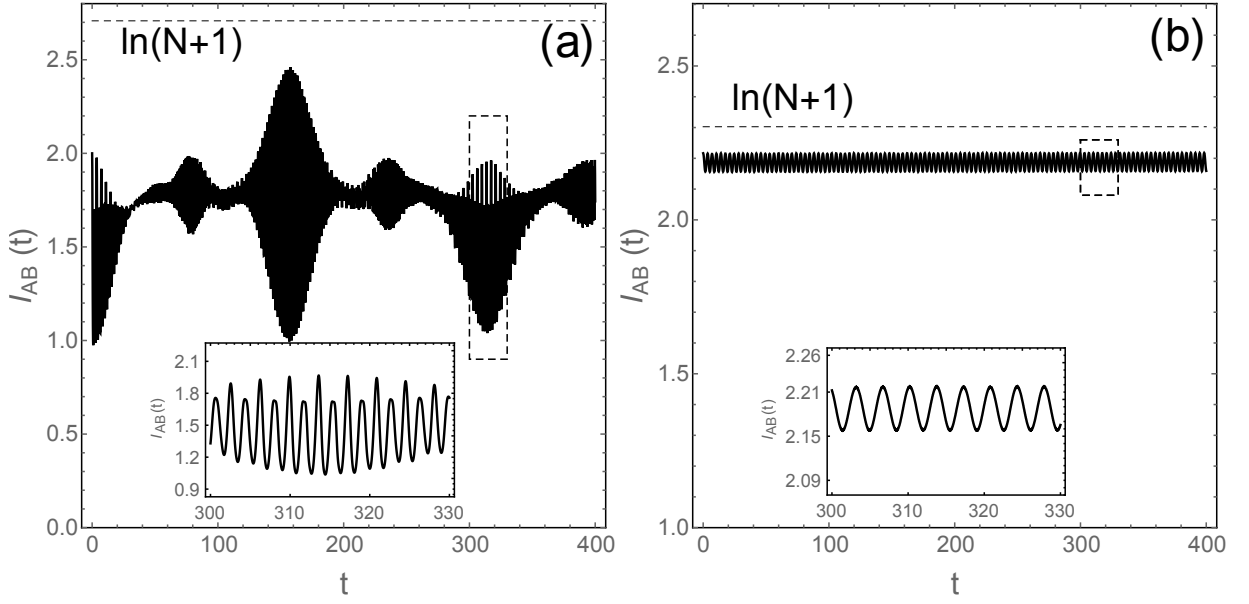


FIG. 10: The dynamical measure of mutual information $I_{A,B}(t)$ for different subspace of (a) $N = 15$ and (b) $N = 10$ with the same parameters as in Fig.8. Insets: the zoomed-in images of $I_{A,B}(t)$ from the dashed rectangles.

where the joint Q -function $Q(\alpha_A, \alpha_B, t)$ and the marginal Q -functions $Q(\alpha_A, t)$, $Q(\alpha_B, t)$ have been given by Eq.(17) and Eq.(20)(21), respectively. The mutual information concerns about the information sharing between two modes with a limit of

$$0 \leq I_{AB}(t) \leq \ln(N+1),$$

where $N+1$ is the dimension of the Hilbert space of \mathcal{H}_N . If the Q -function can separate at a transient time of t_s by satisfying $Q(\alpha_A, \alpha_B, t_s) = Q(\alpha_A, t_s)Q(\alpha_B, t_s)$, then $I_{AB}(t_s) = 0$ and the two modes will be desynchronized at time t_s without sharing any information. This measure implies that QS is somehow related to the quantum entanglement between two modes. For a pure quantum state under unitary evolution, the mutual information can be expressed by

$$I_{AB}(t) = -2 \int Q(\alpha_A, t) \ln Q(\alpha_A, t) \frac{d^2 \alpha_A}{\pi}. \quad (27)$$

By using the marginal Q -function defined by Eq.(20), above mutual information can be calculated by

$$I_{AB}(t) = -4 \int_0^\infty Q(r, t) \ln Q(r, t) dr,$$

where

$$Q(r, t) = e^{-r^2} \sum_{j=0}^N \frac{\Gamma(N-j+\frac{1}{2})}{j!(N-j)!} |C_j(t)|^2 r^{2j}.$$

Fig.10 calculates the dynamics of the mutual information under the same parameters as that in Fig.9 just for a dynamical comparison. We can see, strictly, the mutual information $I_{AB}(t)$, exhibits a different dynamics from that of measure $S_c(t)$. However, both measures indicate correlated dynamics of synchronization with a similar decreasing or increasing fluctuation at the same time as that shown in Fig.8. Although Fig.9 and Fig.10 seem to have opposite mean-value tendencies, their relevant ‘collapse and revival’ behaviors keep close connections. Fig.9 and Fig.10 also show that the fluctuation amplitudes of two different measures depends heavily on the initial states of the whole system (see the trapping case of $N = 10$ is very different from $N = 15$). Furthermore, based on Q -functions, we can see that QS is somehow related to the quantum correlations (e.g., entanglement, discord, mutual entropy) and connected to a mathematical problem of dynamical variable separation for a joint probability function, such as $Q(\alpha_A, \alpha_B, t_s) \rightarrow Q(\alpha_A, t_s)Q(\alpha_B, t_s)$.

B. QS of scattering modes from BEC in a coherent state

As the importance of the initial state of BEC, we now consider QS again for two scattering modes generated from a BEC in a coherent state. In this case, the whole Hilbert space of the system is a direct sum of the subspaces of \mathcal{H}_N with different atomic number of N , and the wave function in the whole Hilbert space $\mathcal{H} = \bigoplus_N \mathcal{H}_N$ should be expanded by

$$|\Psi(t)\rangle = \sum_{N_A, N_B} C_{N_A; N_B} |N_A, N_B\rangle, \quad (28)$$

where the number states of $\hat{N}_{A,B} |N_{A,B}\rangle = N_{A,B} |N_{A,B}\rangle$. Therefore the dynamical coefficients meet

$$\begin{aligned} i\dot{C}_{N_A; N_B} &= [\delta(N_A - N_B) + \chi(N_A^2 + N_B^2 + 4N_A N_B - N_A - N_B)] C_{N_A; N_B} \\ &+ [(g - \chi) + \chi(N_A + N_B)] \sqrt{N_B(N_A + 1)} C_{N_A+1; N_B-1} \\ &+ [(g - \chi) + \chi(N_A + N_B)] \sqrt{N_A(N_B + 1)} C_{N_A-1; N_B+1}, \end{aligned} \quad (29)$$

where the atomic number N_A, N_B of the two modes have no limit in the whole Hilbert space. But within a certain subspace of specific $N = N_A + N_B$, the above Eq.(29) returns back to Eq.(14). By using the coefficients $C_{N_A; N_B}$, $N_{A,B} = 0, 1, 2, \dots$, the phase-space quasi-probability distribution function of $Q(\alpha_A, \alpha_B)$ can be written as

$$Q(\alpha_A, \alpha_B, t) = \left| \sum_{N_A, N_B} C_{N_A; N_B}(t) \frac{(\alpha_A^*)^{N_A} (\alpha_B^*)^{N_B}}{\sqrt{N_A! N_B!}} \right|^2 e^{-(|\alpha_A|^2 + |\alpha_B|^2)},$$

which satisfies $0 \leq Q(\alpha_A, \alpha_B, t) \leq 1$ proved by Cauchy's inequality. As the Q -function $Q(\alpha_A, \alpha_B, t)$ describes the probability distribution of a two-mode state in the phase space, the single-mode quasi-probability distribution function for A or B is obtained by the integral of

$$Q(\alpha_{A,B}, t) = \int Q(\alpha_A, \alpha_B, t) \frac{d^2 \alpha_{B,A}}{\pi}.$$

With polar coordinates of $\alpha_{A,B} = r_{A,B} e^{i\theta_{A,B}}$, the marginal Q -functions for mode A and B can be obtained as

$$\begin{aligned} Q(\alpha_A, t) &= e^{-|\alpha_A|^2} \sum_{N_A, N'_A, N_B} \frac{\Gamma\left(\frac{2N_B+1}{2}\right)}{N_B!} \frac{C_{N_A N_B} C_{N'_A N_B}^*}{\sqrt{N_A! N'_A!}} (\alpha_A^*)^{N_A} (\alpha_A)^{N'_A}, \\ Q(\alpha_B, t) &= e^{-|\alpha_B|^2} \sum_{N_A} \frac{\Gamma\left(\frac{2N_A+1}{2}\right)}{N_A!} \sum_{N_B} \frac{(\alpha_B^*)^{N_B}}{\sqrt{N_B!}} C_{N_A N_B} \sum_{N'_B} \frac{(\alpha_B)^{N'_B}}{\sqrt{N'_B!}} C_{N_A N'_B}^*. \end{aligned}$$

The initial quantum state of the two-mode system in the whole Hilbert space is then assumed to be

$$|\Psi(0)\rangle = |\alpha_0\rangle_A \otimes |0\rangle_B = e^{-|\alpha_0|^2/2} \sum_{j=0}^{\infty} \frac{\alpha_0^j}{\sqrt{j!}} |j, 0\rangle,$$

which means that the coefficients are zero except for $C_{N_A; 0}(0) = e^{-|\alpha_0|^2/2} \frac{\alpha_0^{N_A}}{\sqrt{N_A!}}$, where $N_A = 0, 1, 2, \dots, \infty$. In order for a numerical calculation, we should introduce a specific number of n for a truncated sum of the coefficients

$$C_{N_A; 0}(0) = e^{-|\alpha_0|^2/2} \frac{\alpha_0^{N_A}}{\sqrt{N_A!}}, \quad N_A = 0, 1, 2, \dots, n,$$

which can be simplified further by only choosing $N_A \in [|\alpha_0|^2 - \sqrt{|\alpha_0|^2}, |\alpha_0|^2 + \sqrt{|\alpha_0|^2}]$ because of the initial Poisson population distribution. For convenience, we change the subscripts of $C_{N_A; N_B}$ and use the equations of motion in a closed truncated Hilbert space (because the total atomic number is still conserved) of

$$\begin{aligned} i\dot{C}_{kl} &= [\delta(k-l) + \chi(k^2 + l^2 + 4kl - k - l)] C_{kl} + \sqrt{l(k+1)} [g + (k+l-1)\chi] C_{k+1; l-1} \\ &+ \sqrt{k(l+1)} [g + (k+l-1)\chi] C_{k-1; l+1}, \end{aligned} \quad (30)$$

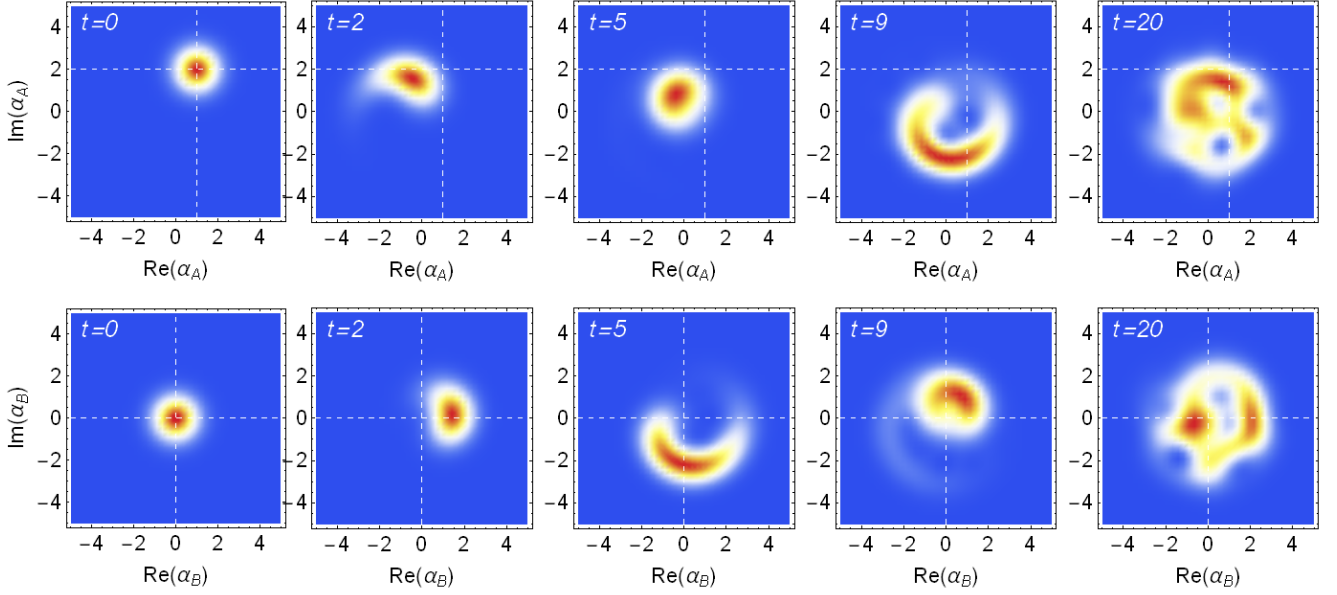


FIG. 11: The temporal distributions of Q -functions for two symmetric modes ($\delta = 0$) of $Q(\alpha_A, t)$ (upper panel) and $Q(\alpha_B, t)$ (lower panel). The dashed lines indicate the central positions of the initial states for modes A and B . The initial state for the mode A is in a coherent state of $|\alpha_0\rangle$ with $\alpha_0 = 1 + 2i$ and the mode B is in a vacuum state $|0\rangle$. The nonlinear coupling rate $\chi/g = -0.01$ and the time unit of evolution is $\pi/[1 + (N - 1)\chi/g]$.

where (k, l) are all the integer pairs satisfying $k + l \leq N$, $N = 0, 1, 2, \dots, n$, and the total number of C_{kl} or equations is $(n + 1)(n + 2)/2$. Therefore, the marginal Q -functions will be

$$Q(\alpha_A, t) = e^{-|\alpha_A|^2} \sum_{k=0}^n \sum_{l=0}^{n-k} \sum_{j=0}^{n-k-l} \frac{\Gamma(k + \frac{1}{2})}{k!} \frac{C_{lk} C_{jk}^*}{\sqrt{l!j!}} (\alpha_A^*)^l (\alpha_A)^j, \quad (31)$$

and

$$Q(\alpha_B, t) = e^{-|\alpha_B|^2} \sum_{k=0}^n \sum_{l=0}^{n-k} \sum_{j=0}^{n-k-l} \frac{\Gamma(k + \frac{1}{2})}{k!} \frac{C_{lk} C_{kj}^*}{\sqrt{l!j!}} (\alpha_B^*)^l (\alpha_B)^j. \quad (32)$$

By using Eq.(30), the distribution patterns of $Q(\alpha_A, t)$ and $Q(\alpha_B, t)$ in the whole Hilbert space \mathcal{H} are shown in Fig.11 with an initial Q -functions being $Q(\alpha_A, 0) = \sqrt{\pi} e^{-(|\alpha_0|^2 + |\alpha_A|^2)} \sum_{i=0}^n \sum_{j=0}^n (\alpha_A^* \alpha_0)^i (\alpha_A \alpha_0^*)^j$ and $Q(\alpha_B, 0) = \sqrt{\pi} e^{-(|\alpha_0|^2 + |\alpha_B|^2)}$. The dynamics of the Q -functions shows that the probability distributions of modes A and B in the phase space can never reach a same pattern at a same time if they starts from different initial states due to the conservations of their respective coherences. However their distribution patterns will come closer to share a common phase space and perform a similar shape variation with a time lag because of the nonlinear couplings between them. Therefore, the synchronized motion of the mode states can be somehow indicated by obtaining similar but complementary patterns in the phase space, especially after a long time evolution (see the last column of Fig.11 for $t = 20$). The different quantum MS in a whole Hilbert space from that in Fig.7 is only due to a broken of the number conservation in one BEC beam within a subspace of \mathcal{H}_N . For an atomic BEC in a coherent state, there are many BEC beams with different atomic numbers of N mixing together during the state evolution in the whole Hilbert space of $\mathcal{H} = \bigoplus_N \mathcal{H}_N$. The nonlinear mechanical modes A and B generated from different BEC beams can coherently mix together via the linear coupling g and the nonlinear coupling χ which give the irregular patterns of the motion probability as shown in Fig.11. According to the symmetry of modes A and B in the scattering process, the same Q distributions of two modes in the phase space will own a lower total energy for Boson modes and thus modes A and B intend to share a same phase area and evolve into a similar distribution pattern indicated by Fig.11.

In the Hilbert space of \mathcal{H} , the dynamics of CS and QS between scattering modes from coherent state BEC will be different from that from number state BEC due to the different dynamics of the mean values and the variances of the

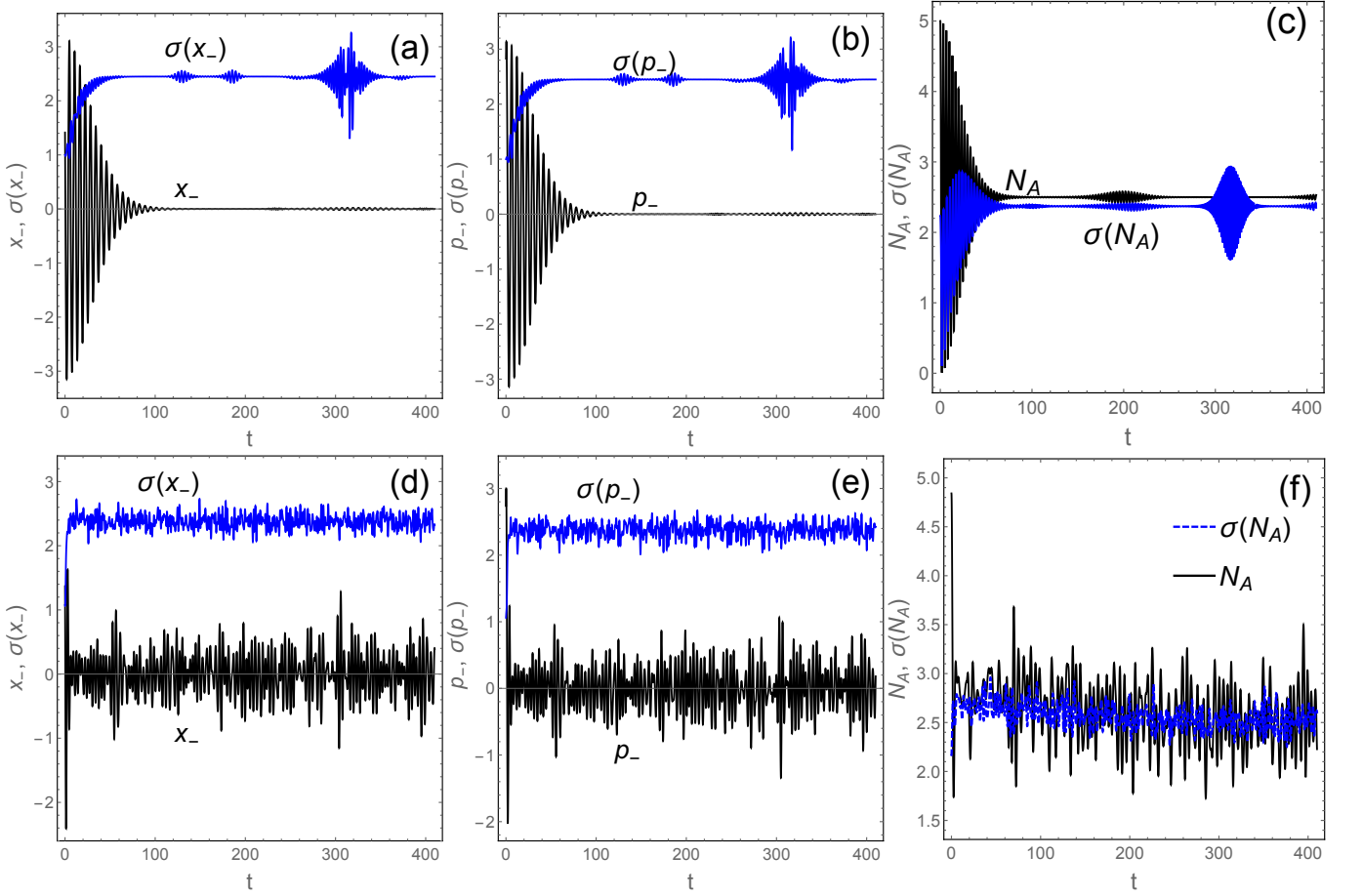


FIG. 12: The dynamics of mean values and their relevant uncertainties in the whole Hilbert space of $\bigoplus_N \mathcal{H}_N$ (a)-(c) for $N = 0, 1, 2 \dots, 15$ and (d)-(f) for $N = 0, 1, 2 \dots, 10$. The other parameters are the same as that in Fig.8.

error operators. In this case, the mode number \hat{N}_A and its variance can be determined by

$$N_A(t) = \langle \hat{a}_A^\dagger \hat{a}_A \rangle = \sum_{k,l} k |C_{kl}(t)|^2, \quad \sigma(N_A) = \sqrt{\sum_{k,l} k^2 |C_{kl}(t)|^2 - \left(\sum_{k,l} k |C_{kl}(t)|^2 \right)^2}.$$

Fig.12 calculates the dynamics of the mean values and their corresponding fluctuations, and it shows that the quantum fluctuations (which are omitted in a classical dynamics) still play an important roles in the synchronized behaviors in this case. For a coherent-state BEC, two scattering modes can quickly reach an exact CS in a sense of $x_- \rightarrow 0, p_- \rightarrow 0$ (see Fig.12 (a)(b)) but their fluctuations present “collapse and revival” behaviors and will remain for a long time due to the weak dissipations of the BEC scattering modes. But for a trapping truncation of $n = 1 - g/\chi \approx 10$, the two modes hardly reach to a complete CS but more irregular fluctuations are produced than that in the number-state BECs (see Fig.8(d)(e)(f)) because two scattering modes generated in the number-state BECs will no longer trap themselves in their initial states within their respective Hilbert space of \mathcal{H}_N and the mode mixing between different number-state BECs will be involved.

Similarly, we investigate the Mari measure of $S_c(t)$ in the mixed Hilbert space by calculating

$$S_c(t) \leq \frac{1}{2\sigma(x_-)\sigma(p_-)} \leq \frac{1}{2},$$

and the Q -function mutual information (Eq.(27))

$$I_{AB}(t) = -\frac{2}{\pi} \int_0^\infty \int_0^{2\pi} Q(r, \theta, t) \ln [Q(r, \theta, t)] dr d\theta, \quad (33)$$

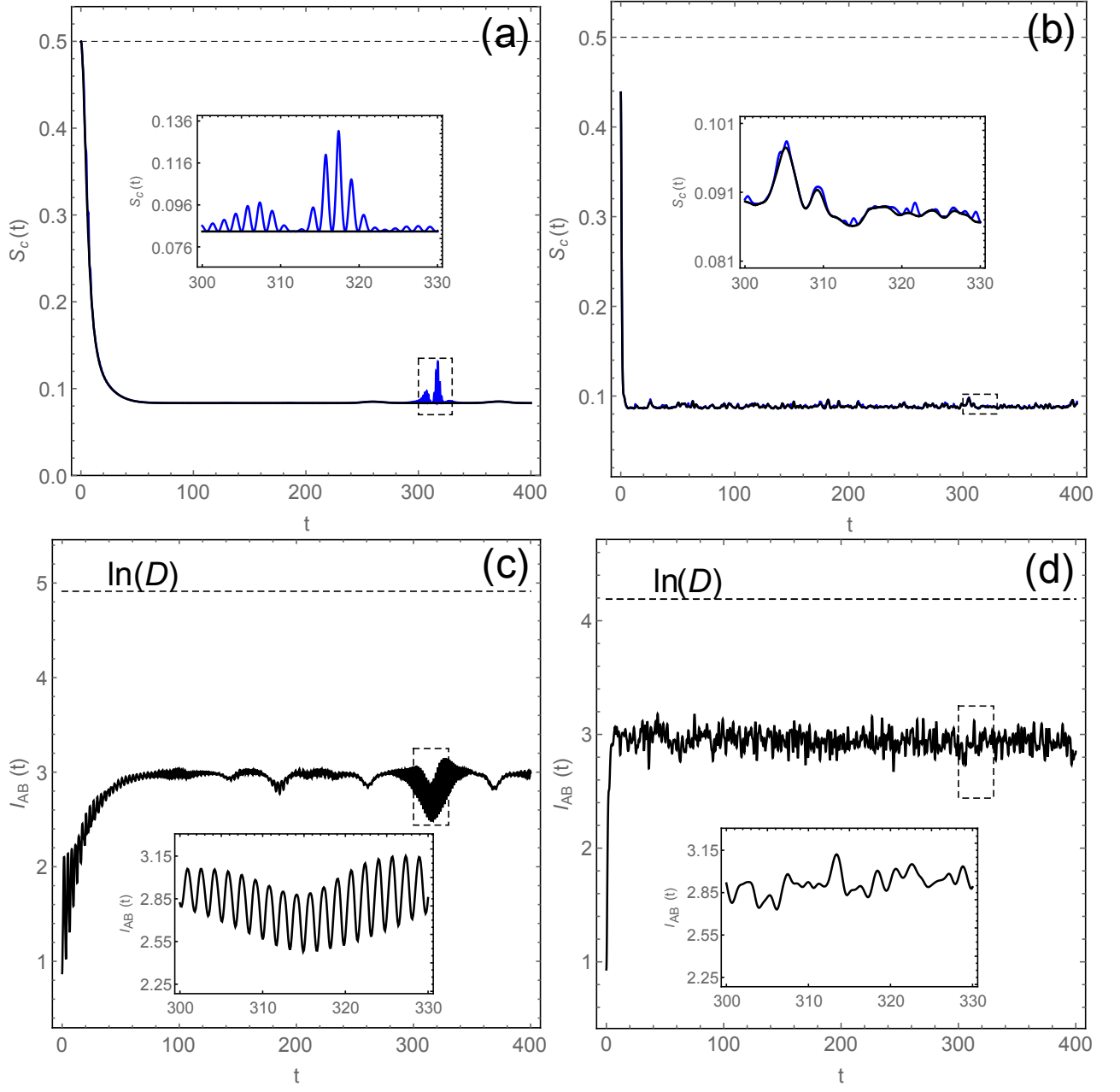


FIG. 13: The dynamical measure synchronization of (a)(b) $S_c(t)$ and (c)(d) the mutual information $I_{AB}(t)$ in the whole Hilbert space of $\bigoplus_N \mathcal{H}_N$ for $N = 0, 1, 2, \dots, n$. The truncated number $n = 15$ for (a) (c) and $n = 10$ for (b)(d). The other parameters are the same as that in Fig.9 and Fig.10. Insets: the zoomed-in images from the dashed rectangles.

where

$$Q(r, \theta, t) = e^{-r^2} \sum_{k=0}^n \frac{\Gamma(k + \frac{1}{2})}{k!} \left[\sum_{l=0}^{n-k} \sum_{j=0}^{n-k} \frac{C_{lk}(t) C_{jk}^*(t)}{\sqrt{l!j!}} r^{l+j} e^{i(j-l)\theta} \right].$$

In this case, the mutual information between the two modes has a limit of $0 \leq I_{AB}(t) \leq \ln D$, where the full dimension of the truncate Hilbert space is $D = (n+1)(n+2)/2$. Both the temporal evolutions of $S_c(t)$ and $I_{AB}(t)$ are comparatively demonstrated in Fig.13(a)-(d). The calculation of the mutual information in this case is a little more complicated because the integral dimension of Q -function in Eq.(33) is doubled with respect to both the amplitude r and the phase θ . According to our calculation, we can see that both Mari measure $S_c(t)$ and mutual information

$I_{AB}(t)$ exhibit smoother characteristics of motion, but their opposite mean-value tendencies and relevant details of “revival and collapse” still indicate a close connection with each other. Anyway, based on the quantum measures expressed by Q -function, we show that the synchronized behaviors between two nonlinear modes in a closed quantum system can exhibit microscopic dynamics of QS by establishing similar irregular patterns in the phase space. The QS measures estimated either by $S_c(t)$ or by $I_{AB}(t)$ are closely connected to the everlasting fluctuations maintained by the quantum correlations during the quantum evolution beyond mean-value dynamics.

V. CONCLUSION

Usually, the synchronization refers to an emergent behavior that often occurs between coupled self-sustained oscillators (the driven dissipative systems) [25, 26] by means of establishing collective correlated dynamics among different autonomous oscillators. However, in a problem of quantum control of quantum units with nonlinear couplings, only the synchronized dynamics beyond decoherence is concerned about, which enables the validity of treating an open system as a closed non-dissipative system. In the closed quantum systems, the synchronized behaviors at macroscopic and microscopic levels both play important roles during the control process and a complete investigation of synchronization for a whole quantum system should include both CS and QS. Therefore, in this paper, we choose BEC as an example to investigate the dynamics of CS and QS between two nonlinear scattering modes both from the classical and quantum points of view. Our study shows that the evolution of two scattering modes exhibits strong synchronized behaviors in both classical and quantum aspects in spite of their nonlinear dynamics. The CS in a closed quantum system is based on the mean-value behavior due to its macroscopic dynamical scale and exhibits a typical phenomenon of MS which gives attractive interwinding trajectories in the phase space sharing similar phase areas because of the conservation of total phase volume and the equilibrium energy exchange between modes. We propose a comparable method to use Q -function as a tool to study the corresponding QS behavior and investigate the dynamics of QS through the overlapping patterns of probability density in the phase space as well as the mutual information sharing between two nonlinear modes. The calculations reveal that the “revival and collapse” of the fluctuations, derived from the coherent superposition of eigenmodes (see Eq.(13) or Eq.(28)), discriminates the dynamics of QS from CS, and a full synchronization for CS is basically impossible for QS in a closed system. The calculation indicates that the overlaps of the correlated trajectories established in CS are statistically different from that of the similar density patterns characterized in QS.

In order to highlight the roles of quantum fluctuations in the synchronization, the Mari measure of $S_c(t)$, which is a generalized measure of CS based on the dynamical variances (e.g. $\sigma(x)$ and $\sigma(p)$)[12], is calculated in the quantum regime. The result indicates that the upper limitation of $S_c(t)$, which excludes an exact synchronization between two non-dissipative quantum modes, is due to the permanent fluctuations of the unitary evolutions of a closed quantum system, and the dynamics of fluctuations is hence sensitively dependent on the initial states of the system (e.g. number state BEC or coherent state BEC). In the other hand, the QS measure estimated by the mutual information $I_{AB}(t)$ gives similar dynamics of the fluctuations compared with that of $S_c(t)$ in spite of the opposite mean time dynamical tendencies of decreasing $S_c(t)$ and increasing $I_{AB}(t)$ starting from the same initial states. The evolution of the mutual information calculated by Q -function also implies a close connection of QS with the quantum entanglement [31] in a sense of variable separation of Q -functions. The synchronized behavior of a closed quantum system analyzed by Q -function reveals that the distance measure of $S_c(t)$ and the correlation measure of $I_{AB}(t)$ are dynamically equivalent in spite of providing different aspects of synchronization, and which further implies that the measure to describe QS can not be uniquely defined as that for CS.

Anyway, based on the different measures calculated by Q -function, we can find that the synchronized behaviors between two nonlinear modes in a closed quantum system exhibit not only the macroscopic behaviors of CS by establishing interwinding trajectories in the classical phase space, but also the microscopic behaviors of QS by conducting similar dynamics of irregular distribution patterns in the quantum phase space. The QS measures estimated either by the distance variance $S_c(t)$ or by the mutual information $I_{AB}(t)$ are connected with each other by a relevant dynamics of fluctuation beyond the mean-value dynamics. As the intrinsic fluctuations related to quantum correlations are perfectly protected in a closed quantum system, the uncertainty principle inevitably excludes the complete synchronization for QS and basically discriminates the QS from CS.

Acknowledgments

This work is supported by the National Natural Science Foundation of China (Grants No.11447025 and No.11234003) and the National Basic Research Program of China (973 Program) under Grant No. 2011CB921604.

-
- [1] C. Brif, R. Chakrabarti and H. Rabitz, *Control of quantum phenomena: past, present and future*, New J. Phys. **12**, 075008 (2010).
- [2] H. Wiseman, *Quantum Measurement and Control*, Cambridge: Cambridge University Press, 2010.
- [3] M. Bagheri, M. Poot, M. Li, W.P.H. Pernice, and H.X. Tang, *Dynamic manipulation of nanomechanical resonators in the high-amplitude regime and non-volatile mechanical memory operation*, Nat. Nanotech. **6**, 726 (2011).
- [4] S.B. Shim, M. Imboden, and P. Mohanty, *Synchronized Oscillation in Coupled Nanomechanical Oscillators*, Science **316**, 95 (2007).
- [5] L. Ying, Y.C. Lai, C. Grebogi *Quantum manifestation of a synchronization transition in optomechanical systems*, Phys Rev A, **90** 053810 (2014).
- [6] P.P. Orth, D. Roosen, W. Hofstetter, K.L. Hur, *Dynamics, synchronization, and quantum phase transitions of two dissipative spins*, Phys Rev B, **82** 144423 (2010).
- [7] M.R. Hush, Weibin Li, Sam Genway, Igor Lesanovsky, and Andrew D. Armour, *Spin correlations as a probe of quantum synchronization in trapped-ion phonon lasers*, Phys. Rev. A, **91** 061401(R) (2015).
- [8] C.A. Holmes, C.P. Meaney, and G.J. Milburn, *Synchronization of many nanomechanical resonators coupled via a common cavity field*, Phys. Rev. E **85**, 066203 (2012).
- [9] K. Shlomi, D. Yuvaraj, I. Baskin, O. Suchoi, R. Winik, E. Buks *Synchronization in an optomechanical cavity*, Phys Rev E, **91** 032910 (2015).
- [10] G. Heinrich, M. Ludwig, J. Qian, B. Kubala, and F. Marquardt, *Collective Dynamics in Optomechanical Arrays*, Phys. Rev. Lett. **107**, 043603 (2011).
- [11] M. Zhang, G.S. Wiederhecker, S. Manipatruni, A. Barnard, P. McEuen, and M. Lipson, *Synchronization of Micromechanical Oscillators Using Light*, Phys. Rev. Lett. **109**, 233906 (2012).
- [12] A. Mari, A. Farace, N. Didier, V. Giovannetti, and R. Fazio, *Measures of Quantum Synchronization in Continuous Variable Systems*, Phys. Rev. Lett. **111**, 103605 (2013).
- [13] V. Ameri, M. Eghbali-Arani, A. Mari, A. Farace, F. Kheirandish, V. Giovannetti, and R. Fazio, *Mutual information as an order parameter for quantum synchronization*, Phys. Rev. A **91**, 012301 (2015).
- [14] I. Goychuk, J. Casado-Pascual, M. Morillo, J. Lehmann and P. Hönggi, *Quantum Stochastic Synchronization*, Phys. Rev. Lett. **97**, 210601 (2006).
- [15] O.V. Zhirov and D.L. Shepelyansky, *Synchronization and Bistability of a Qubit Coupled to a Driven Dissipative Oscillator*, Phys. Rev. Lett. **100**, 014101 (2008).
- [16] D.K. Agrawal, J. Woodhouse and A.A. Seshia, *Observation of Locked Phase Dynamics and Enhanced Frequency Stability in Synchronized Micromechanical Oscillators*, Phys. Rev. Lett. **111**, 084101 (2013).
- [17] T.E. Lee and H.R. Sadeghpour, *Quantum Synchronization of Quantum van der Pol Oscillators with Trapped Ions*, Phys. Rev. Lett. **111**, 234101 (2013).
- [18] M.H. Matheny, Matt Grau, L.G. Villanueva, R.B. Karabalin, M.C. Cross and M.L. Roukes, *Phase Synchronization of Two Anharmonic Nanomechanical Oscillators*, Phys. Rev. Lett. **112**, 014101 (2014).
- [19] S. Walter, A. Nunnenkamp and C. Bruder, *Quantum Synchronization of a Driven Self-Sustained Oscillator*, Phys. Rev. Lett. **112**, 094102 (2014).
- [20] J. Gieseler, M. Spasenović, L. Novotny and R. Quidant, *Nonlinear Mode Coupling and Synchronization of a Vacuum-Trapped Nanoparticle*, Phys. Rev. Lett. **112**, 103603 (2014).
- [21] H.P. Breuer and F. Petruccione, *The Theory of Open Quantum Systems*, Oxford University Press, New York (2007); K. H. Hughes, *Dynamics of Open Quantum Systems*, CCP6, Warrington UK (2006).
- [22] G.L. Giorgi, F. Galve, G. Manzano, P. Colet, and R. Zambrini, *Quantum correlations and mutual synchronization*, Phys. Rev. A **85**, 052101 (2012).
- [23] G.M. Xue, M. Gong, H.K. Xu, W.Y. Liu, H. Deng, Y. Tian, et al. *Observation of quantum stochastic synchronization in a dissipative quantum system*, Phys Rev B, **90** 224505 (2014).
- [24] Weiping Zhang, D. F. Walls, *Bosonic-degeneracy-induced quantum correlation in a nonlinear atomic beam splitter*, Phys. Rev. A **52**, 4696 (1995) .
- [25] A. Balanov, N. Janson, D. Postnov, and O. Sosnovtseva, *Synchronization: From Simple to Complex* (Springer-Verlag, Berlin, 2009).
- [26] A. Pikovsky, M. Rosenblum and J. Kurths, *Synchronization: a universal concept in nonlinear sciences*, Cambridge University Press, Cambridge UK (2001).
- [27] S. Boccaletti, J. Kurths, G. Osipov, D. L. Valladares, and C. S. Zhou, *The synchronization of chaotic systems*, Phys. Rep. **366**, 1 (2002).
- [28] S. M. Barnett, J. A. Vaccaro, *The Quantum Phase Operator: A Review*, CRC Press, Taylor Francis (2007).
- [29] A. Hampton and D. H. Zanette, *Measure Synchronization in Coupled Hamiltonian Systems*, Phys. Rev. Lett. **83**, 2179

- (1999).
- [30] H. Qiu, B. Juliá-Díaz, M. A. Garcia-March, and A. Polls, *Measure synchronization in quantum many-body systems*, Phys. Rev. A **90**, 033603 (2014).
 - [31] G. Manzano, F. Galve, G. L. Giorgi, E. Hernández-García and R. Zambrini, *Synchronization, quantum correlations and entanglement in oscillator networks*, Sci. Rep. **3**, 1439 (2013).
 - [32] Lin Zhang, *Opto-mechanical estimation of micro-trap with cold atoms via nonlinear stimulated Raman scattering spectrum*, Appl. Phys. B: Lasers and Optics, **111**, 195 (2013).
 - [33] A. Smerzi, S. Fantoni, S. Giovanazzi, and S. R. Shenoy, *Quantum Coherent Atomic Tunneling between Two Trapped Bose-Einstein Condensates*, Phys. Rev. Lett. **79**, 4950 (1997).
 - [34] U. E. Vincent, *Measure synchronization in coupled Duffing Hamiltonian systems*, New J. Phys. **7**, 209 (2005).
 - [35] Wen-Yuan Wang, Jie Liu, and Li-Bin Fu, *Measure synchronization in a spin-orbit-coupled bosonic Josephson junction*, Phys. Rev. A **92**, 053608 (2015).
 - [36] Jing Tian, Haibo Qiu, Guanfang Wang, Yong Chen, and Li-bin Fu, *Measure synchronization in a two-species bosonic Josephson junction*, Phys. Rev. E **88**, 032906 (2013).
 - [37] W. Barth, R. S. Martin and J. H. Wilkinson, *Calculation of the Eigenvalues of a Symmetric Tridiagonal Matrix by the Method of Bisection*, Numerische Mathematik, **9**, 386 (1967).